Is there an effect of Bay of Bengal salinity on the northern Indian Ocean climatological rainfall?

K. S. Krishnamohan, Jérôme Vialard, Matthieu Lengaigne, Sébastien Masson, Guillaume Samson, Stéphane Pous, Suresh Neetu, Fabien Durand, S. S. C. Shenoi, Gurvan Madec

Accepted Manuscript

Is there an effect of Bay of Bengal salinity on the northern Indian Ocean climatological rainfall?

K.S. Krishnamohan, J. Vialard, M. Lengaigne, S. Masson, G. Samson, S. Pous, S. Neetu, F. Durand, S.S.C. Shenoi, G. Madec

PII: S0967-0645(18)30132-2

DOI: https://doi.org/10.1016/j.dsr2.2019.04.003

Reference: DSRII 4568

To appear in: *Deep-Sea Research Part II*

Received Date: 9 June 2018

Revised Date: 27 March 2019

Accepted Date: 1 April 2019

Please cite this article as: Krishnamohan, K.S., Vialard, J., Lengaigne, M., Masson, S., Samson, G., Pous, S., Neetu, S., Durand, F., Shenoi, S.S.C., Madec, G., Is there an effect of Bay of Bengal salinity on the northern Indian Ocean climatological rainfall?, *Deep-Sea Research Part II* (2019), doi: https://doi.org/10.1016/j.dsr2.2019.04.003.

Is there an effect of Bay of Bengal salinity on the Northern Indian Ocean climatological rainfall?

KS. Krishnamohan[1], J. Vialard[1], M. Lengaigne[1,2], S. Masson[1], G. Samson[3], S. Pous[1,6], S. Neetu[4], F. Durand[3], S.S.C Shenoi[5], G. Madec[1]

[1] Sorbonne Universités (UPMC, Univ Paris 06)-CNRS-IRD-MNHN, LOCEAN Laboratory, IPSL, Paris, France
[2] Indo-French Cell for Water Sciences, IISc-NIO-IITM–IRD Joint International Laboratory, NIO, Goa, India
[3] IRD/Laboratoire d'études en Géophysique et Océanographie Spatiales (LEGOS), Toulouse, France
[4] National Institute of Oceanography, Goa, India.
[5] Indian National Centre for Ocean Information Services, Hyderabad, India
[6] Department of Oceanography, University of Cape Town, South Africa

Corresponding author:
Krishnamohan K.S
LOCEAN - Case 100
Case 100 - Université P. et M. Curie
4, Place Jussieu - 75252 Paris Cedex 05
FRANCE
Email: krishmet@gmail.com

Abstract

The northern Bay of Bengal (BoB) receives a large amount of freshwater directly from monsoonal rains over the ocean, and indirectly through river runoffs. It has been proposed that the resulting strong salinity stratification inhibits vertical mixing of heat, thus contributing to maintain warm sea surface temperature and high climatological rainfall over the BoB. In the present paper, we explore this positive feedback loop by performing sensitivity experiments with a 25-km resolution regional coupled climate model, that captures the main BoB features reasonably well. We confirm that salinity stratification tends to stabilize the upper ocean, thereby increasing the mixed layer warming due to vertical mixing by ~+0.5°C.month^{-1} on annual average. Salinity however also induces a compensating cooling by altering the mixed layer heating rate by air-sea heat fluxes, so that the net effect on climatological surface temperature is negligible. During and shortly after the southwest monsoon, this compensation predominantly occurs through increased cooling by upward latent heat fluxes. During boreal winter, it occurs because salinity favours a thinner mixed layer, which is more efficiently cooled by negative air-sea heat fluxes. These compensations result in a negligible climatological surface temperature and rainfall change at all seasons. This weak influence of salinity stratification on climatological surface temperature and rainfall in our model is robust when applying a flux correction to alleviate model biases, when neglecting the solar absorption below the mixed layer and when using different atmospheric radiation and convective parameterizations.

1. Introduction

With 60% of jobs in the agriculture sector, the livelihood of the densely-populated Indian subcontinent crucially depends on the Indian summer monsoon rainfall (Webster et al., 1998; Gadgil and Gadgil, 2006), which accounts for about 90% of annual precipitation over India. During boreal summer, the differential heating between the Asian landmass and the ocean to the south sets up a low pressure area over south Asia reinforced by the elevated heating on the Tibetan plateau (Li and Yanai, 1996). The dynamical response to this pressure gradient consists of a low-level and large-scale cross-equatorial flow (Joseph and Raman, 1966; Findlatter, 1969), which induces surface evaporation and collects moisture over the Indian Ocean. From June to September, the northern branch of this flow results in strong southwesterly winds over the Arabian Sea (AS) and the associated moisture transport is then flushed over the Indian subcontinent and Bay of Bengal (BoB) (Findlater, 1969).

This strong south-west monsoon rainfall and the associated larger riverine input (mainly from the Ganges-Brahmaputra and Irrawaddy) results in a large freshwater input into the BoB during the southwest monsoon, with rainfall accounting for more than two thirds (e.g. Sengupta et al., 2006; Akhil et al., 2014; Chaitanya et al., 2014). This large freshwater input into a relatively-small, semi-enclosed basin yields some of the lowest climatological Sea Surface Salinities (SSS) in the tropical band (Chaitanya et al., 2014), with a maximum freshening in the top 10-40 meters, resulting in a sharp near-surface salinity stratification, especially in the northern BoB (e.g. Vinayachandran et al., 2002; Behara and Vinayachandran, 2016; Sengupta et al., 2016). This salinity stratification has a strong stabilizing effect on the upper ocean, maintaining a shallow mixed layer (Mignot et al., 2007; Girishkumar et al., 2013) and often resulting in the formation of a barrier layer, i.e. a salinity-stratified layer between the bottom of the mixed layer and top of the thermocline (Lukas and Lindstrom, 1991; Sprintall and Tomczak, 1992). Barrier layers usually appear during summer in the eastern BoB and mature during winter both in amplitude and spatial extent, covering the entire northern BoB (Rao and Sivakumar, 2003; Thadathil et al., 2007; Kumari et al., 2018; Li et al., 2017).

The barrier layer impacts the mixed layer temperature heat budget, by isolating the warm surface layer from the colder upper thermocline and preventing the entrainment of cold subsurface water into the mixed layer (Vialard and Delecluse, 1998). The salinity stratification within the barrier layer can even support temperature inversions (i.e. warmer water below than within the mixed layer, e.g. Han et al., 2001; Girishkumar et al., 2013; Thadathil et al., 2016). In

presence of such temperature inversions, entrainment (that usually cools the mixed layer) can even warm the surface layer during winter (de Boyer Montegut et al., 2007). The strong salinity stratification thus appears to play a key role in maintaining a relatively high Sea Surface Temperature (SST) in the BoB by reducing the vertical mixing of heat during and after the southwest monsoon (de Boyer Montegut et al., 2007).

In a seminal study, Shenoi et al. (2002) proposed that the vertical salinity stratification in BoB could contribute to a coupled ocean-atmosphere positive feedback loop that maintains intense climatological rainfall regionally. In this hypothesis, summarized on the sketch of Fig. 1, a strong rainfall and river freshwater forcing yields a low SSS and strong vertical salinity stratification in the BoB (Step I on the Fig. 1). This strong, stable salinity stratification (and the associated barrier layer) inhibits the cooling of the mixed layer by turbulent mixing at its bottom, maintaining SST above 28.5°C during the entire summer monsoon (Step II on Fig. 1). Such SST above 28.5°C is a necessary condition for deep atmospheric convection to occur (Gadgil et al., 1984; Graham and Barnett, 1987), thus allowing to maintain regional rainfall and runoffs (Step III on Fig. 1) and completing the feedback loop. Shenoi et al. (2002) supported this hypothesis by the analysis of observational climatologies, that indicate that the available mixing energy from the wind is not sufficient to overcome the stabilizing effect of the salinity stratification. The feedback loop proposed by Shenoi et al. (2002) could thus contribute to maintain a high climatological rainfall over the BoB.

The Shenoi et al. (2002) hypothesis is not only important to understand the present-day BoB climatological rainfall, but may also be very relevant in the context of anthropogenic climate change. Climate models and theoretical arguments indeed support an intensification of the hydrological cycle as the troposphere warms in response to increasing greenhouse gases concentrations (e.g. Held and Soden, 2006). The observational records already detect an intensification of salinity contrasts as a result, *i.e.* increasing salinities in regions dominated by evaporation, and decreasing salinities in high rainfall regions, including in the BoB (e.g. Durack and Wijfels, 2010). The Shenoi et al. (2002) hypothesis, if correct, would provide an additional positive feedback mechanism to further enhance the climate change impact on rainfall regionally in the Bay of Bengal region. This provides an additional motivation to investigate the validity of this hypothesis thoroughly.

Ocean modelling experiments have explored the consequences of the BoB salinity stratification before (Han et al., 2001; Howden and Murtugudde, 2001; Behara and

Vinayachandran, 2016). Han et al. (2001) used a reduced-gravity ocean model and found that the effect of freshwater fluxes was dominated by the effect of river runoffs and resulted in a localised ~0.5-1°C surface warming in the northwestern BoB in summer, in response to the Kelvin wave forced by the Ganges-Brahmaputra river inflow. Howden and Murtugudde (2001) used a reduced gravity primitive equation model and only found a very local impact of river discharge on BoB summer SST, confined to nearest grid points to the Ganges-Brahmaputra and Irrawady river mouths, and more widespread ~0.5°C cooling in the northeastern BoB during winter. In a recent study using an ocean general circulation model, Behara and Vinayachandran (2016) found that freshwater fluxes induced a ~0.5°C warming in the northwestern BoB during summer, and 0.5 to 1.5°C cooling in the eastern BoB during both summer and winter.

None of the studies above however represents deep atmospheric convection explicitly, a key element in the Shenoi et al. (2002) hypothesis (Fig. 1). A recent study with a coupled general circulation model (Vinayachandran et al., 2015) suggests that river runoffs contribute to a 10% decrease of Indian summer rainfall, opposite to what should be expected from Shenoi et al. (2002) hypothesis. This study however switched off river runoffs not only in the BoB but at a global scale, and finds really modest SST changes in the BoB (~ 0.2°C). It is therefore possible that the Indian monsoon change in this study is rather associated with the remote response to large SST signals in the northern Pacific and Atlantic Ocean (>2°C). The most relevant coupled model study of the Shenoi et al. (2002) hypothesis is thus that of Seo et al. (2009), using a fully coupled regional circulation model. This study mimics freshwater fluxes into the BoB by applying a relaxation to SSS climatology, which makes the SSS much lower in the BoB as compared to their reference experiment. This increased salinity stratification however resulted in a very weak salinity-induced surface warming in the northwestern BoB in summer (~0.2°C), and a weak atmospheric response.

So far, the hypothesis of Shenoi et al. (2002) is thus not clearly supported by existing numerical experiments. On the one hand, ocean modelling studies (Han et al., 2001; Howden and Murtugudde, 2001; Seo et al., 2009; Behara and Vinayachandran, 2016) do not resolve potential atmospheric feedbacks associated with deep atmospheric convection changes. On the other hand, existing coupled model studies find rainfall changes that are either negligible (Seo et al., 2009) or opposite to what is expected from the Shenoi et al. (2002) hypothesis (Vinayachandran et al., 2015). For these reasons, we aim to revisit this hypothesis using a state-of-the-art regional coupled model that captures the main features of the Indian Ocean mean climate, including the

146 monsoon, and its time-variability (Samson et al., 2014). We will do so by comparing reference
147 experiments with sensitivity experiments in which we neglect the influence of salinity on vertical
148 mixing (as in e.g. Vialard and Delecluse, 1998). Section 2 describes the model, the observational
149 datasets, the experimental design and the mixed layer temperature budget. Section 3 provides a
150 validation of the simulated BoB climatological features, focusing on the key processes involved
151 in Shenoi et al. (2002) hypothesis. Section 4 discusses the influence of salinity stratification on
152 BoB climate, for both summer and winter. We will also show that our results are robust
153 irrespective of whether we apply a flux correction or not to alleviate model biases, and for
154 different choices of oceanic and atmospheric parameterizations. A summary and discussion of
155 our results are finally presented in Section 5.
156

157 ## 2. Model and methods

158 ### 2.1. Model configuration

159 We use a regional coupled model to assess the influence of the BoB salinity stratification
160 on the northern Indian Ocean climate. This model couples the NEMO (Nucleus for European
161 Modelling of the Ocean) oceanic (Madec et al., 2008) and the WRF (Weather Research and
162 Forecasting Model) atmospheric (Skamarock and Klemp, 2008) primitive equation models
163 through the OASIS3 coupler (Valcke, 2013), and is named NOW for NEMO-OASIS-WRF.

164 We use a very similar Indian Ocean configuration to the one extensively described and
165 validated in Samson et al. (2014), and therefore only provide a brief summary of this
166 configuration in the following. This model is applied to the Indian Ocean sector (25.5^{o}E-
167 142.25^{o}E, 34.5^{o}S-26^{o}N), with the oceanic and atmospheric component sharing the same 1/4° (~25
168 km) horizontal grid. The ocean component has 46 vertical levels, with a resolution ranging from
169 6 m to 18 m in the upper 100 m. The atmospheric component has 28 sigma vertical levels, with a
170 higher resolution of 30 m near the surface. Variable lateral boundary conditions are supplied from
171 a global simulation for the oceanic component (Brodeau et al., 2010), and from the ERA-Interim
172 reanalysis (Dee et al., 2011) for the atmosphere. River runoffs are prescribed from the Dai and
173 Trenberth (2002) climatological river product. This dataset includes the two major rivers flowing
174 into the BoB (Ganges-Brahmaputra and Irrawady that collectively represent ~80% of the total
175 river runoffs into the BoB) but also smaller rivers such as the Krishna, Godavari, and Mahanadi.

The ocean model parameterizations include a turbulent kinetic energy scheme for vertical mixing (Blanke and Delecluse, 1993). It uses a monochromatic formulation of the penetrative solar irradiance following a single exponential profile, with an e-folding depth scale set to 23 m corresponding to a Type I water in Jerlov's (1968) classification (oligotrophic waters). This parameterization is in line with recent observational estimates for the BoB (Lotliker et al., 2016). Atmospheric model physics include the Betts-Miller-Janjic (BMJ) scheme (Janjic, 1994) for subgrid-scale convection, the WRF single-moment six-class microphysics scheme WSM6 (Hong and Lim, 2006), the Dudhia (1989) shortwave radiation scheme, the Rapid Radiation Transfer Model (RRTM) for longwave radiation (Mlawer et al., 1997), the Yonsei University planetary boundary layer (Noh et al., 2003) and the four-layer Noah land surface model (Chen et al., 1996).

The present model setup differs from the simulations discussed in Samson et al. (2014) as the WRF model version has been updated from its version 3.2 to 3.3.1 and Dudhia (1989) shortwave radiation scheme has been preferred to the one of Goddard (Chou and Suarez, 1999). In line with the model version discussed in Samson et al. (2014), the reference simulation from the present configuration shares a lot in common with the one presented in Samson et al. (2014). Although an exhaustive validation of the present model configuration is out of the scope of this paper, a validation of the main model parameters involved in the feedback loop hypothesized by Shenoi et al. (2002) will be provided in Section 3.

2.2. Experimental design

The reference model simulation is referred to as the control run (CTL hereafter). This 18-year simulation was forced at the boundaries using conditions from the 1990-2007 period. The initial conditions on the 1st January 1990 are provided from ERA-Interim reanalysis data for the atmospheric component and from the ¼° ocean simulation described in Brodeau et al. (2010) for the ocean. Additional sensitivity experiments were performed over the same period to test the impact of haline stratification on the BoB climate. They are listed in Table 1 and described below.

Vertical mixing is parameterized using a turbulent kinetic energy closure scheme (Blanke and Delecluse, 1993) in our CTL. Using a similar strategy to Vialard and Delecluse (1998) and Masson et al. (2005), we conduct a "NOS" sensitivity experiment. This experiment is identical to "CTL", except that the vertical mixing is resolved assuming a constant salinity of 35 pss in the [5°S-25°N; 65°E-105°E] region (dashed blue frame on Fig. 3d) which encompasses the BoB and South-Eastern AS, where the seasonal export of BoB freshwaters induces a somewhat similar

behaviour to that in the BoB (e.g. de Boyer Montégut et al., 2007; Vinayachandran et al., 2007). The computation of vertical mixing is smoothly transitioned to fully accounting for the effects of salinity within 5° of the edges of this region. The NOS minus CTL experiment will thus specifically isolate effects of the salinity stratification in the BoB region on the regional climate, hence allowing to test the feedback loop hypothesized by Shenoi et al. (2002).

As we will see in more details in section 3, the CTL simulation strongly overestimates the wind stresses over the BoB, which yields a too deep mixed layer, too thin barrier layer and underestimated salinity stratification. Since the realism of the haline stratification is critical to our results, we performed a wind stress-corrected reference experiment FCTL (see Table 1), in which the wind stress provided to the ocean model was multiplied by a factor of 0.5 within the [8°N - 26°N, 76°E -100°E] region, with a smooth transition within 6° of the edges. Penetrative solar heat flux has a significant influence on the SST seasonal evolution in the BoB (e.g. de Boyer Montegut et al., 2007). We will demonstrate in section 3 that this flux correction approach strongly reduces the mixed layer depth (MLD) and barrier layer thickness (BLT) biases in the CTL experiment, and will further present our results based on FCTL and a twin experiment that neglects the effect of salinity stratification on vertical mixing (FNOS) in section 4. We will demonstrate in section 4 that our results are robust irrespective of whether the flux correction is applied or not.

Since our results could also be sensitive to some choices in physical parameterizations, we have also redone twin set of experiments similar to CTL and NOS with various choices. Howden and Murtugudde (2001) have shown that different SST anomalies develop in response to river inputs, depending on whether solar radiation is allowed to penetrate into the ocean or not. In order to test the sensitivity of our results to penetrative solar flux, we perform twin experiments for CTL and NOS, where the solar penetration is disabled and the entire solar flux is absorbed within the top model level (CTL_NSP and NOS_NSP experiments). Deep atmospheric convection is an essential component of Shenoi et al. (2002) hypothesis, and the results presented here may be sensitive to the convective scheme. The sensitivity of our results to the choice of convective scheme will thus be addressed by comparing results obtained using the BMJ moist convective adjustment scheme, with those obtained using the updated Kain-Fritsch (KF) atmospheric convective scheme (Kain, 2004) (CTL_KF and NOS_KF experiments). Similarly, the sensitivity of our results to the shortwave radiation scheme in experiments with the Goddard scheme (Chou and Suarez, 1999), previously employed in Samson et al. (2014) (CTL_G and

NOS_G experiments). As we will see, our results on the effect of the BoB haline stratification on climatological rainfall are robust in any set of twin experiments above.

2.3. Mixed layer temperature budget.

The processes controlling SST are characterized using an online mixed layer heat budget (Vialard and Delecluse, 1998; Vialard et al., 2001). The equation for the average temperature over the time-varying mixed layer T_{ml} (a proxy for SST) reads as follows:

$$\partial T_{ml} = \underbrace{-\frac{1}{h}\int_{-h}^{0} u\partial_x T dz - \frac{1}{h}\int_{-h}^{0} v\partial_y T dz}_{\text{horizontal advection}} - \underbrace{\frac{1}{h}\int_{-h}^{0} D_l(T)}_{\text{lateral process}}$$

$$\underbrace{-\frac{1}{h}(T_{ml} - T_{-h})(w_{-h} + \partial_t h) - \frac{1}{h}[K_z \partial_z T]_{-h}}_{\text{subsurface vertical process}} + \underbrace{\frac{Q_s(1-F_{-h})+Q_{ns}}{\rho_0 C_p h}}_{\text{atmospheric forcing}(F_T)} \quad (1)$$

The first two terms on the RHS respectively represent zonal and meridional temperature advection in the mixed layer, where h is the time-varying model mixed layer estimated based on a potential density increase of 0.01 kg m^{-3} relative to the density at 10-m depth and (u, v, w) are the components of the current. The second term on the RHS represents lateral mixing processes, $D_l(T)$ being model horizontal diffusion operator: this term will not be discussed in the following as it is always negligible in the present analysis. The third term on the RHS gathers the vertical exchanges of heat between the mixed layer and the subsurface ocean, including the effects of upwelling w_{-h} (T_{-h} − T_{ml}), entrainment $\partial_t h$ (T_{-h} − T_{ml}) (computed as a residual from all the other terms) and turbulent mixing at the bottom of the mixed layer K_z ∂_z T_{-h}, where K_z is the vertical mixing coefficient for tracers. The last term on the RHS represents the atmospheric heat flux forcing, Q_s and Q_{ns} being respectively the solar and non-solar components of the surface heat flux, F_{-h} the fraction of incoming solar radiation that penetrates down to the depth h, ρ_0 the seawater reference density, and C_p the sea water volumic heat capacity.

2.4. Validation datasets

The model SST and rainfall climatologies distribution are validated against the Tropical Rainfall Measuring Mission (TRMM) Microwave Imager (TMI) dataset (http://www.remss.com/tmi). The ERA-interim dataset (Dee et al., 2011) is used to validate the wind at 10 m and air-sea heat and momentum fluxes are validated using the Tropflux product (Praveen Kumar et al., 2012, 2013).

The ocean model climatological salinity and temperature distributions are validated against the North Indian Ocean Atlas (NIOA) (Chatterjee et al., 2012) dataset. The model MLD and BLT are compared with the observationally-derived climatology of de Boyer Montegut (2004) (http://www.ifremer.fr/cerweb/deboyer/mld/home.php). In order to be strictly comparable to this product, the model MLD and isothermal layer depth (ILD, with BLT=ILD-MLD) are computed from 5-day averaged model temperature and salinity. We use the same criteria as in de Boyer Montegut (2004), i.e. a 0.2°C increase relative to 10-m depth temperature for ILD, and an equivalent density increase (on average 0.065 kg m^{-3} for typical BoB temperature, salinity conditions) relative to 10-m depth density for MLD. The BLT estimate is anyway robust when computed with either the de Boyer Montégut (2004) criterion or the 0.01 $kg.m^{-3}$ criterion used for diagnosing the surface layer heat budget. Li et al. (2017) have found (their figure 5) that the BLT climatology diagnosed from the WOA13 dataset (which is similar to the NIOA atlas we use) is very similar to diagnosing this BLT from individual Argo profiles, suggesting that our approach for constructing our BLT validating dataset is reasonable.

3. Model validation

This section provides a brief validation of the reference (CTL) and flux-corrected (FCTL) simulations. The model climatology is always computed over the entire 18-years of the simulations. We will validate BoB-averaged climatologies of important parameters in the Shenoi et al. (2002) hypothesis, and demonstrate that the FCTL experiment compares better with observations. Finally, we will show the surface mixed layer heat budget in the FCTL experiment, which will allow to qualitatively check the consistency with previous studies.

3.1. Testing the validity of the wind stress correction approach

Fig. 2 shows the climatological seasonal cycle of several BoB-averaged parameters that are important for testing Shenoi et al. (2002) hypothesis (SST, SSS, wind and wind stress, rainfall, net heat flux, haline stratification measured through MLD and BLT). Observationally-derived wind and wind stress are strongest during the southwest monsoon over the BoB, with a secondary maximum associated with the northeast monsoon in December-January (Fig. 2a,b). Rainfall is maximum in July during the southwest monsoon (Fig. 2c). Net air-sea heat fluxes into the ocean are largest before the monsoon, close to zero during the southwest monsoon, and become negative during the northeast monsoon (Fig. 2h). This seasonal heat flux evolution is generally consistent with the evolution of SST trend. SST is indeed warmest in the BoB in April-May

297 before the southwest monsoon (Fig. 2d) and coolest in January-February during the northeast
298 monsoon. The strong monsoon rainfall (Fig. 2c) and river runoffs yield lowest salinities in
299 October right after the southwest monsoon (Fig. 2e). The MLD has a clear semi-annual cycle
300 with shallowest MLD during the inter-monsoon seasons, and deeper MLD during both monsoons
301 (Fig. 2f), due to enhanced wind stirring (in summer) and negative air-sea fluxes (in winter). The
302 barrier layer is thickest in boreal winter, i.e. after the southwest monsoon (Fig. 2g).

303 The control simulation generally reproduces the phase of the observed seasonal cycle quite
304 well, but has several marked biases. First, the model wind stress is strongly overestimated all year
305 long (by ~80% on average; see Fig. 2a). In contrast, the model wind speed is overestimated (by
306 15% on average; see Fig. 2b). However, this overestimation also combines with a 20%
307 overestimation of the wind variance (the June to September BoB-averaged CTL wind speed
308 variance is 4.5 $m.s^{-1}$ vs. 3.7 $m.s^{-1}$ for ERA-I). The quadratic dependence of the wind stress on the
309 wind velocity magnifies these two modest biases and results in a strong wind stress
310 overestimation over the BoB. Rainfall is also overestimated by ~55% in summer over the BoB in
311 the CTL experiment (Fig. 2c). Net heat flux into the ocean also exhibits a negative bias (Fig. 2h),
312 larger from March to October (~20 $W.m^{-2}$) mainly due an overestimated latent heat flux as a
313 consequence of the overestimated wind speed (not shown). The net heat flux bias is in line with
314 the ~1°C too cold model SST (Fig. 2d). Despite the overestimated oceanic rainfall, the SSS is too
315 salty (Fig. 2e) and the MLD too deep (Fig. 2f) all year-long in the CTL experiment. This is
316 probably because the much too strong wind stress induces too much near-surface mixing. This
317 intense wind stirring also yields a too thin barrier layer (Fig. 2g), especially in winter (the
318 January-February average BLT is ~23 m in CTL vs. ~35 m in observations). The biases discussed
319 above are of the same order or smaller than the ones in the previous coupled studies that tested
320 the Shenoi et al. (2002) hypothesis.

321 We attempted to reduce those biases by applying an ad-hoc wind stress correction in the
322 FCTL experiment. Fig. 2a shows that our strategy of the modifying wind stress is successful in
323 producing a much more realistic wind stress seasonal cycle (Fig. 2a). It also considerably
324 improves the haline stratification, confirming that the too strong wind stirring was the main cause
325 of this bias. Applying the flux correction indeed results in a strong reduction of the MLD bias all
326 through the year (Fig. 2f). It also corrects the salty SSS bias found in CTL, with SSS in FCTL
327 that even becomes fresher than observations (Fig. 2e). The barrier layer bias is also reduced, with
328 a thickness that is very close to observations in January-July and even overestimated by 5 to 10 m

from August to December. It must however be noted that this wind-stress correction has little impact on the rainfall (Fig. 2c) and SST (Fig. 2d) systematic biases, which already suggests a weak impact of salinity stratification on climatological SST and rainfall. This will be confirmed by all the set of twin experiments discussed later in the paper.

Given that FCTL exhibits a more realistic salinity stratification (although slightly overestimated) as compared to CTL, we will present results derived from this experiment in the rest of section 3 and in most of section 4. We will discuss the possible effect of FCTL remaining biases (too cold BoB, too strong rainfall, slightly overestimated haline stratification) on our results in section 5.

3.2. Winter and summer simulated climate

In this subsection, we will mainly focus on summer (June to September, hereafter JJAS) and winter (December to March, hereafter DJFM). Summer is the focus of Shenoi et al. (2002) and is characterized by the strongest BoB freshwater forcing. We will also discuss winter, for which salinity stratification impacts the BoB climate most in the only available regional coupled model study (Seo et al., 2009).

Despite the rainfall overestimation illustrated by Fig. 2c, the FCTL experiment generally reproduces the observed seasonal rainfall and wind climatologies (not shown). To quantify this, we compute pattern correlations discussed hereafter which were calculated with respect to the observational climatologies mentioned in section 2.4 for the northern Indian Ocean region (0°-25°N; 40°E-100°E). This pattern correlation reaches 0.84 (summer) and 0.94 (winter) for rainfall and 0.93 (summer) and 0.92 (winter) for wind speed. The FCTL simulation also captures seasonal SST patterns very well (0.90 pattern correlation for summer and 0.93 for winter), despite the general tendency to underestimate the SST by about ~1°C seen in Fig. 2d.

Fig. 3 provides a more thorough validation of the BoB SSS (colours) and BLT (a proxy for the vertical stratification, contours). The strong freshwater fluxes arising from the summer oceanic precipitation and continental runoffs result in a strong freshening (with SSS as low as 30 pss) in the northern and eastern part of the BoB in summer (Fig. 3a), where river runoff and oceanic precipitation are most intense, with saltier waters to the south. During summer, barrier layer only develops in the eastern BoB (contours on Fig. 3a). During winter, the SSS distribution remains roughly consistent to that in in summer (with fresher water to the North), but with less intense meridional SSS gradients (Fig. 3b). In winter, observations indicate 20 to 30 m thick barrier layers develop in the northern BoB (contours on Fig. 3b) and expand into the southeastern

AS. The model reproduces the observed SSS patterns very well (a pattern correlation of 0.97 for JJAS and 0.98 for DJMF), with low salinity in the northern and eastern BoB and saltier water to the south and in the AS in both summer and winter. The model also qualitatively reproduces the observed barrier layer distribution (0.80 pattern correlation in summer and 0.81 in winter), with barrier layers mainly located in the eastern BoB in summer and thicker, more widespread barrier layers in the south-eastern AS and BoB in winter. It must however be noted that the model BLT is underestimated in the northern BoB in winter (up to 40 m in observations against 25 to 30 m in the model), which could be related to the model thermohaline biases in this region, whose possible impacts will be further discussed in section 5.2.

3.3. Simulated seasonal upper-ocean heat balance

To investigate the Shenoi et al. (2002) hypothesis with confidence, we need to assess whether the upper ocean thermal heat balance (that controls the SST) is qualitatively similar in our model to what was described from previous observational and modelling studies. Fig. 4 provides the mean seasonal cycle of the mixed layer heat budget terms (described in section 2.3) averaged over the BoB, along with the MLD and surface net heat flux components.

From February to April, the total tendency is positive (Fig. 4a) and associated to rising SST before the monsoon (Fig. 2d). This heating tendency is driven by the positive net air-sea heat fluxes result from a combination of (1) increased shortwave radiation (Fig. 4b) due to the northward migration of the sun during spring and low nebulosity before the monsoon and (2) reduced latent heat fluxes (Fig. 4b) due to the mild winds at this time of the year (Fig. 2b). This warming by the atmospheric forcing is partially counterbalanced by vertical processes (Fig. 4a), which tend to cool the ocean surface by promoting mixing with deeper, cooler water. The advection terms are relatively weak when averaged over the entire BoB.

The SST first cools slightly at the beginning of the summer monsoon (May to July, Fig. 2d). The initial cooling is largely the result of a strong decrease of the heating by atmospheric heat fluxes (Fig. 4a), which does not balance the cooling through vertical processes any more. The weaker warming by air-sea fluxes is due to both a reduction of incoming solar radiation (due to the strong nebulosity) and relatively strong latent heat fluxes (Fig. 4b) associated with the strong winds at this season (Fig. 2b). Towards the end of the monsoon (August to September), the warming tendency due to surface net heat fluxes is almost balanced by the cooling by vertical processes (Fig. 4a), and SST does not vary much in that period (Fig. 2d).

From October to January, the BoB cools (Fig. 2d and Fig. 4a). This cooling is driven by negative surface net heat fluxes (Fig. 4b) in response to reduced incoming solar radiation due to the southward migration of the sun and increased latent heat loss (Fig. 4b) due to northeast monsoon winds (Fig. 2b). The longwave fluxes also contribute to the negative neat heat fluxes during winter months, because of a less humid atmosphere and weaker greenhouse effect. During that period, the mixed layer deepens (Fig. 2f) and oceanic vertical processes act to warm the surface layer and to damp the heat flux winter cooling (Fig. 4a). This warming by vertical mixing and entrainment of subsurface waters is due to the presence of temperature inversion during that season in the BoB in the model, as in observations (e.g. Thadatil et al., 2016).

This heat balance agrees qualitatively well with that presented from a forced model framework in figure 3c of de Boyer Montégut et al. (2007): the BoB SST changes are flux-driven with subsurface processes acting as a moderating factor. Both analyses also suggest a significant role of the haline stratification in maintaining relatively high SSTs in the BoB: during winter, vertical mixing and entrainment actually warm the surface layer due to the presence of a salinity-sustained temperature inversion.

4. Influence of salinity on Bay of Bengal Climatological Rainfall

The analyses in section 3 suggest that the FCTL simulation captures the main climatological features of the northern Indian Ocean seasonal cycle for the key parameters involved in the Shenoi et al. (2002) hypothesis. The model in particular reproduces a warming tendency by oceanic vertical mixing and entrainment during winter, which could not happen in the absence of salinity stratification, and hence temperature inversion below the mixed layer. In the following subsections, we will first investigate how salinity influences exchanges of heat between the mixed layer and deeper ocean (section 4.1), before assessing its overall effect on climatological SST and rainfall (section 4.2). In section 4.3, we will demonstrate that the results obtained from the flux corrected experiments (FCTL and FNOS) are robust without the flux correction, and with several different choices of physical parameterisations.

4.1. Salinity reduces the vertical mixing of heat in the Bay of Bengal

We first perform a consistency check to ascertain that the difference between FCTL and FNOS experiments indeed captures the expected oceanic impact of the salinity stratification. Fig. 5a,c shows that the salinity stratification induces a shallower MLD everywhere in the BoB and

eastern AS. This salinity-induced MLD shoaling reaches 5.5 m in summer and 10.1 m in winter when averaged over the BoB. In the "NOS" experiments, the MLD is only sensitive to the thermal stratification, i.e. there is no barrier layer (Vialard and Delecluse, 1998). As expected, the salinity-induced MLD deepening pattern matches the barrier layer thickness pattern in the FCTL run, with largest ML deepening in regions where the barrier layers are thickest (contours on Fig. 5). The pattern correlation between FNOS-FCTL MLD difference and FCTL BLT is indeed 0.86 in JJAS and 0.95 in DJF. This analysis illustrates that the salinity effects assessed from FCTL minus FNOS are physically consistent.

Upper ocean salinity stratification strengthens the upper ocean stability in the BoB and eastern AS, and limits the downward mixing of heat. Fig. 5b,d shows the FCTL minus FNOS climatology of the mixed layer heating rate through vertical mixing (cf. equation 1). As expected, this difference is positive in regions where a barrier layer is present in FCTL. In regions where a temperature inversion is present, there is a warming by vertical processes in FCTL (cf section 3.3), while there can only be a cooling by vertical processes in FNOS, where no temperature inversions can be sustained. In regions where no temperature inversion is present, the cooling by vertical processes is decreased in FCTL relative to FNOS, due to the insulating effect of the barrier layer. As a result, the salinity influence on vertical mixing always favours a warming of the mixed layer in regions where a barrier layer is present in FCTL (Fig. 5b,d). This salinity-induced warming through vertical mixing is not, in principle, only controlled by the barrier layer thickness distribution, but also by the salinity gradient across the barrier layer, temperature stratification below, and wind stirring. There is however an overall reasonable correspondence between the FCTL barrier layer thickness and salinity-induced change in turbulent heat fluxes at the bottom of the mixed layer, especially in winter (pattern correlation of 0.47 for JJAS and 0.81 for DJFM).

Overall, the BoB salinity stratification inhibits vertical mixing, and contributes to a $+0.5°C.month^{-1}$ enhancement of the mixed layer heating rate by vertical mixing during JJAS and $+0.44°C.month^{-1}$ during DJFM. This impact of salinity stratification on the vertical mixing term is thus consistent with the Shenoi et al. (2002) hypothesis (Step II on Fig. 1) and other previous studies (de Boyer Montegut et al., 2007; Behara and Vinayachadran, 2016).

4.2. Compensating effects yield a weak impact of salinity stratification on SST and rainfall

Fig. 6 quantifies the climatological differences in BoB average SST and rainfall between FNOS and FCTL. The simulated summer SST (Fig. 6a) and rainfall (Fig. 6b) climatologies are almost identical in those simulations. Maps (not shown) likewise reveal very weak local rainfall, wind and surface temperature changes, which are generally not statistically significant, including on continents. In other words, the Shenoi et al. (2002) hypothesis does not seem to operate in our model, i.e. the salinity stratification does not seem to influence the SST or rainfall climatology. As we discussed above, however, salinity stratification contributes to an anomalous ~2°C mixed layer warming through vertical mixing over the summer monsoon (i.e. 0.5°C.month^{-1} during 4 months). Our simulations are thus consistent with the step II of the Shenoi et al. (2002) hypothesis on Fig. 1 (cf. Section 4.1). The absence of any significant climatological SST change however indicates that other processes compensate the salinity-induced warming through vertical mixing, yielding a weak impact on climatological SST (step III), and thus no impact on freshwater forcing through ocean-atmosphere coupling (step I). In the rest of this subsection, we will explain why there is no SST change despite the strong salinity-induced anomalous surface warming by vertical mixing.

Fig. 7a shows the BoB-average FCTL minus FNOS mixed layer heat budget climatology, i.e. the salinity contribution to the SST balance. In line with the analysis shown on Fig. 5c,d, the salinity stratification contributes to a mixed layer warming through vertical mixing (blue curve on Fig. 7a), in particular during and after the summer monsoon. However, this warming tendency by subsurface processes is almost entirely balanced by a cooling tendency by atmospheric forcing (orange curve on Fig. 7a). This almost equal compensation between the salinity-induced surface layer heating by vertical mixing and cooling by atmospheric forcing results in an almost nil total SST tendency (Fig. 7a) and therefore very similar SSTs in the FCTL and FNOS experiments (Fig. 6a).

Several processes can lead to the change in the atmospheric forcing term seen on Fig. 7a. This term reads as follows:

$$\frac{Q_S(1-\mathcal{F}_{-h})+Q_{NS}}{\rho_0 C_P h} \qquad (2)$$

First, a change in one or several components of the surface heat flux (solar Q_s and non-solar Q_{ns} surface fluxes) can alter the net heat flux entering into the ocean and modulate the amplitude of the atmospheric forcing term. Second, a change in the MLD impacts the atmospheric forcing term by either modulating the heat capacity of the mixed layer ($\rho_0 C_P h$ at the denominator of

equation 2) or by regulating the fraction of solar flux that penetrates below the mixed layer (F_{-h} in equation 2). Fig. 7c allows estimating those effects separately. The red curve on Fig. 7c is an offline re-computation of FCTL minus FNOS term in equation (2). It does not match exactly the orange curve on Fig. 7a due to the offline computation with 5-day average rather than instantaneous values, but captures its general evolution. The blue curve on Fig. 7c shows this difference, but neglecting the effect of changes in surface fluxes (see Annex A for details). The orange curve neglects the effects of the mixed layer heat capacity changes, and the green curve those of solar penetration. When a coloured curve departs from the red curve, it indicates that salinity influences the heating rate of the mixed layer through that particular effect (see Annex A for details).

Fig. 7c shows that the influence of each of these effects is seasonally-dependent. For instance, there is a clear and dominant effect of salinity on the surface forcing heating rate through the mixed layer heat capacity from November to January (see yellow shading on Fig. 7c). In contrast, changes of surface fluxes contribute most to the atmospheric forcing change from March to October. Below, we will separately discuss the November to January (dominant effect of mixed layer heat capacity) and June to October (dominant effect of changes in air-sea fluxes) periods.

The barrier layer is thickest in the model (and observations) from November to February (Fig. 2g), and this is also the season when salinity contributes to the strongest shoaling of the mixed layer (Fig. 7b). Net surface heat fluxes are negative during this period (Fig. 2h) and contribute to cool the oceanic mixed layer (orange curve on Fig. 4a). By making the mixed layer shallower during this period, salinity reduces its heat capacity and allows a larger cooling rate in response to negative surface heat fluxes. During November to January, salinity thus does not change SST because the warming it induces through its effect on vertical mixing is compensated by a cooling due to negative surface heat fluxes being trapped over a shallower mixed layer.

During June to October, the salinity-induced anomalous cooling is dominated by the effect of a surface net heat flux reduction. Air-sea heat fluxes are indeed different in the FCTL and FNOS experiments (Fig. 7d), with latent heat fluxes dominating those differences during this period. A more detailed analysis (not shown) indicates that latent heat flux increases due to a slightly warmer SST and slightly stronger surface winds in the FCTL experiment. Although those mean SST and wind change are small, they are sufficient to explain the change in latent heat flux, because the Clausius-Clapeyron relation implies an exponential increase of the latent heat fluxes

with background SST, and hence a strong sensitivity of latent heat fluxes to those variables at the BoB high climatological SSTs. Overall, the slightly larger SST and winds in the FCTL simulation contribute to increase upward latent heat fluxes during and shortly after the southwest monsoon, largely cancelling the effect of salinity-induced warming by vertical processes.

4.3. Robustness of the results

Overall, the FCTL and FNOS experiments suggest that salinity stratification favours an anomalous warming of the surface layer through vertical mixing, but that this warming is compensated by a salinity-induced cooling of the surface layer by air-sea fluxes. As a result, the SST (and consequently the rainfall) hardly changes due to salinity stratification effects in the FNOS experiment. In this section, we will investigate the robustness of those results, by investigating the differences in BoB SST and rainfall climatological seasonal cycle in a series of twin-experiments similar to FTCL and FNOS, but no flux correction and different choices in terms of physical parameterizations (cf section 2.2).

Fig. 8a,b shows the mean seasonal cycle of the BoB SST and rainfall in the CTL and NOS experiments (i.e. as FCTL and FNOS, but without a flux correction). Although this experiment has a quite different mean state to the FCTL experiment, with a saltier SSS, deeper MLD and thinner BLT, there is also an almost negligible impact of salinity stratification on the BoB SST and rainfall in this experiment. Fig. 8c,d shows a similar experiment to CTL (i.e. with no flux correction), but where solar heat flux is not allowed to penetrate into the ocean, likewise yield almost no change in climatological SST and rainfall. This illustrates that ignoring solar penetration or considering it does not change the climatological SST or rainfall. Similarly, sensitivity experiments similar to CTL and NOS, but with a different shortwave radiative scheme (Fig. 8e,f) or convective parameterization (Fig. 8g,h) also suggest a very minor impact of the haline stratification on both SST and rainfall. Overall, our coupled model results are insensitive to whether or not we apply a flux correction, consider or not the penetration of solar heat flux, or to a change of the parameterization of two important atmospheric physical processes in the problem that we consider.

5. Summary and discussion

5.1. Summary

The monsoonal rains feed the northern BoB with a large quantity of freshwater, from oceanic rain and river runoffs. This results in some of the lowest surface salinities in the tropical band. Shenoi et al. (2002) proposed that the resulting very strong vertical salinity stratification is involved in a positive feedback loop that sustains intense rainfall in this region. This feedback loop would act as follows. The strong vertical salinity stratification inhibits the vertical mixing of heat. This contributes to maintaining SST above the ~28.5°C threshold for deep atmospheric convection, hence contributing to intense rain above the BoB, which closes the positive feedback loop.

In the present paper, we explore the Shenoi et al. (2002) hypothesis in a 25-km resolution regional coupled climate model. An 18-year long reference experiment was run and validated. The model reproduces the main features of the northern Indian Ocean mean climate in both summer and winter, including the warming of the surface layer through vertical mixing associated with the thick barrier layer and temperature inversions during and after the monsoon. It however tends to produce 50% too strong wind stress, too deep mixed layer and too thin barrier layer when run without flux correction. We largely reduce those biases in a flux-corrected experiment where wind stress is artificially reduced over the BoB. We will discuss possible caveats associated with remaining model biases (in particular a 15% overestimation of wind speed and 1°C SST cold bias over the BoB) in section 5.2.

The role of salinity stratification is then evaluated in a sensitivity experiment in which vertical mixing is computed based on the thermal stratification only (i.e. the haline stratification is neglected). Differences between the wind-stress corrected control experiment and this sensitivity experiment allow evaluating the effect of salinity stratification on the northern Indian Ocean mean climate. Through the analysis of the surface layer heat budget, we find that salinity stratification indeed tends to warm the mixed layer through vertical mixing, during both summer and winter, as hypothesized by Shenoi et al. (2002). Based on observations, Shenoi et al. (2002) predicted an increase in SST and corresponding changes in precipitation related to this mixed layer warming. However, in our experiments, which resolve atmospheric feedbacks, salinity induces a compensating cooling through two distinct mechanisms. During early winter (from November to January), this salinity-induced cooling is of oceanic origin. Salinity indeed induces a thinner, lower heat-capacity mixed layer that cools more in response to the negative air-sea fluxes during this season. During late summer (from July to October), the salinity-enhanced cooling by surface heat-fluxes is dominated by changes in air-sea fluxes. During and shortly after

579 the southwest monsoon, salinity induces more heat losses through latent heat fluxes at the ocean
580 surface, due to slightly warmer SST and stronger winds.

581 Because of these compensating effects on the upper ocean heat budget, salinity does not
582 influence the BoB climatological SST and rainfall in our simulations. This result is very robust,
583 as it is preserved in other sets of sensitivity experiments without the flux correction; without a
584 penetration of solar heat fluxes into the ocean; and with a different parameterization of
585 atmospheric convection or shortwave fluxes. In the next subsection, we discuss our results
586 against previous studies, their robustness, and how they may be affected by model biases.

587 **5.2. Discussion**

588 Below, we will start by comparing our results with those of previous studies, for winter and
589 summer. We will then discuss caveats of the present study.

590 Let us start by comparing our results with other studies for winter. In their 4-layers
591 reduced-gravity model, Han et al. (2001) found little effect of neither rainfall nor river runoffs on
592 the winter BoB SST. Howden and Murtugudde (2001) found an overall 0.5 to 1°C cooling of the
593 Northern BoB in winter, in response to adding river runoffs, but this model has SSS biases of up
594 to 3 pss relative to the Levitus climatology in winter (their plate 2). Behara and Vinayachandran
595 (2016) also found that rivers led to an SST cooling during the entire year along the eastern and
596 northern rim of the BoB, due to winter cooling by atmospheric fluxes projecting onto a thinner
597 mixed layer. Seo et al. (2009) find a cooling over the entire northern BoB in their regional
598 coupled model in winter due to the same process. The difference between our results and those of
599 Seo et al. (2009) and Behara and Vinayachandran (2016) for winter SST arises from a different
600 balance between two competing processes. Those two studies find, as we do, that salinity reduces
601 the winter mixed layer depth, leading to a more efficient cooling by atmospheric fluxes. In
602 contrast with those two studies, we find that – as hypothesized by Shenoi et al. (2002) – salinity
603 stratification also reduces the vertical mixing of heat at the bottom of the mixed layer, with an
604 overall negligible effect on the surface layer heat budget due to this compensation. While the
605 studies by Han et al. (2001) and Howden and Murtugudde (2001) respectively suffered from a
606 very simplified modelling framework and large biases, the last three studies have comparable
607 resolutions, physical parameterizations and biases, making it difficult to conclude which one is
608 the most realistic, and calling for more studies with other coupled models.

609 For summer, Han et al. (2001) found a weak impact of both rainfall and river runoffs on
610 SST. Howden and Murtugudde (2001) found a very localised impact of the river runoff near the

Ganges-Brahmaputra mouth. We won't discuss Behara and Vinayachandran (2016), for which the influence of river runoff on summer SST is due to changes during winter. As in our case, Seo et al. (2009) found very little changes in SST and rainfall at the BoB scale during summer. We find a large impact of salinity on vertical mixing of heat as in several previous studies, but with little impact on SST due to a compensating change in air-sea fluxes. Except for Howden and Murtugudde (2001), there is therefore overall a stronger consensus about salinity not bringing any SST change in summer amongst previous studies although the underlying mechanisms may be different.

Let us now discuss some caveats of our study. With ¼ degree grid spacing, our ocean model is eddy-permitting but not eddy-resolving. This may be an issue, because the BoB has a relatively strong eddy kinetic energy (EKE; e.g. Chelton et al., 2011) generated from remote wind forcing and ocean internal instability (Chen et al., 2018), and eddy may contribute to the SST balance through their influence on upper ocean heat transport. Comparison with altimeter estimates (not shown) however indicate a reasonable representation of the EKE in the BoB, with an underestimation of less than 15%.

Despite the fact to the model used in the present study is amongst one of the best state-of-the-art coupled models for its representation of the northern Indian Ocean climate (Samson et al., 2014) or when compared to the study of Seo et al. (2009), it is not exempt from biases. Even the flux-corrected experiment tends to have a too low surface salinity due to too strong rainfall (Fig. 2c,e) and a ~ 1°C too cool SST all year long (Fig. 2d). Let us briefly discuss the impact of those biases. As displayed on Fig. 9, the salinity stratification is overestimated in FCTL and underestimated in CTL as compared to observationally-derived climatologies, yet the two experiments give similar results (no impact of this salinity stratification on the climatological SST and rainfall), suggesting that this bias has little impact on our results. Observed SSS climatologies however generally underestimate the northern BoB freshening because of the scarcity of salinity measurements in this region as suggested by the very fresh surface signals reported by recent measurements from moored buoys (Sengupta et al., 2016; Wijesekera et al., 2016) and satellite observations (Fournier et al., 2017). Validating the model vertical salinity profile to the northernmost RAMA mooring in the BoB (15°N) indeed suggest that FCTL exhibits a small surface salty bias SSS and a deeper than observed halocline (Fig. 9). Both experiments also tend to underestimate the temperature stratification below ~ 50 m. These biases

of temperature and salinity profiles could result in an underestimation of the effect of salinity on the vertical turbulent heat fluxes.

There is a ~ 1°C cold SST bias in our model setup (Fig. 2d). This bias is partly related to the 15% wind speed overestimation in the BoB (Fig. 2b), which leads to an overestimated evaporative cooling. This ~1°C cold bias could significantly impact our results. In observations, SST is above the observed 28.5°C threshold for deep atmospheric convection (dashed line on Fig. 2d) from March to November, and is very close to this threshold in July-September, implying a strong sensitivity to a potential small SST change. In contrast, the model is below this threshold from July to March (i.e. during most of the southwest monsoon). Figure 10 compares the relation between daily SST and rainfall over the BoB in the model and observations. Observed rainfall is most likely at ~ 29°C, with a large increase of strong rainfall rates occurrence between 28°C and 29°C. In the model, this "switch" to the convective regime occurs at lower SST, between 27 and 28°C. i.e. the model has a 1°C cold SST bias, but its convective threshold is also 1°C cooler than in observations. For this reason, we believe that the cold bias over the BoB in the model does not strongly affect our results.

Acknowledgements

The authors thank IFCPAR (Indo French Centre for Promotion of Advanced Research), New Delhi for funding of the 4907-1 proposal, CNES for funding the SeaLevelALK proposal and the LEFE/EC2CO program for funding of the AO2015-873251 proposal. The simulations used in this study were performed on resources provided by PRACE Research Infrastructure resources CURIE at TGCC, France. We also thank IRD (Institut de Recherche pour le Developpement) for the financial support of the Indo-French collaboration on Indian Ocean research. This is NIO contribution number XXXX.

667 **Annex A: processes responsible for the change in the effect of atmospheric heat fluxes**
668
669 The heating rate of the mixed layer by atmospheric heat flux forcing reads as follows:

$$\frac{Q_S(1-\mathcal{F}_{-h})+Q_{NS}}{\rho_0 C_P h}(a)$$

670 The red curve on fig.7c shows the difference between this term in the control experiment
671 (designated by a c superscript) and "NOS" experiment (designated by a n superscript):

$$\Delta=\frac{{Q_S}^c(1-\mathcal{F}_{-h^c})+{Q_{NS}}^c}{\rho_0 C_P h^c}-\frac{{Q_S}^n(1-\mathcal{F}_{-h^n})+{Q_{NS}}^n}{\rho_0 C_P h^n}(b)$$

672 This term can become large due to several processes. First, a change in one or several
673 components of the surface heat flux can alter the net heat flux entering into the ocean (solar Q_s
674 and non-solar Q_{ns} surface fluxes) and modulate the amplitude of the atmospheric forcing term.
675 This effect can be evaluated by comparing Δ to the term Δ_{flux} below:

$$\Delta_{flux}=\frac{{Q_S}^c(1-\mathcal{F}_{-h^c})+{Q_{NS}}^c}{\rho_0 C_P h^c}-\frac{{Q_S}^c(1-\mathcal{F}_{-h^n})+{Q_{NS}}^c}{\rho_0 C_P h^n}(c)$$

676 The computation above neglects changes in Q_S and Q_{NS}. When Δ is different from Δ_{flux}, it means
677 that the contribution of changes in fluxes matter. A similar strategy is used to identify the effects
678 of two other processes. A change in the MLD h impacts the atmospheric forcing term in two
679 ways. On the one hand, it modulates the heat capacity of the mixed layer $\rho_0 C_P h$ at the
680 denominator of equation (2): a thicker mixed layer is for example less responsive to a given heat
681 flux. This effect is identified by comparing Δ to the term Δ_{hc} below:

$$\Delta_{hc}=\frac{{Q_S}^c(1-\mathcal{F}_{-h^c})+{Q_{NS}}^c}{\rho_0 C_P h^c}-\frac{{Q_S}^n(1-\mathcal{F}_{-h^n})+{Q_{NS}}^n}{\rho_0 C_P h^c}(d)$$

682 On the other hand, the MLD modulates the fraction of solar flux that penetrates below the mixed
683 layer (F_{-h} of last term in equation 1): a thicker mixed layer intercepts more of the incoming solar
684 heat flux (i.e. $1-\mathcal{F}_{-h}$ is larger) than a thin mixed layer. This effect is identified by comparing Δ to
685 the term Δ_{sp} below:

$$\Delta_{sp}=\frac{{Q_S}^c(1-\mathcal{F}_{-h^c})+{Q_{NS}}^c}{\rho_0 C_P h^c}-\frac{{Q_S}^n(1-\mathcal{F}_{-h^c})+{Q_{NS}}^n}{\rho_0 C_P h^n}(c)$$

686 Fig. 7c shows the seasonal climatology of Δ, Δ_{flux}, Δ_{hc}, and Δ_{sp}.

687 **References**

688 Akhil, V.P., Durand, F., Lengaigne, M., Vialard, J., Keerthi, M.G., Gopalakrishna, V.V., Deltel,
689 C., Papa, F., de Boyer Montégut, C., 2014. A modeling study of the processes of surface
690 salinity seasonal cycle in the Bay of Bengal. J. Geophys. Res. Oceans 119, 3926-3947.
691 doi:10.1002/2013JC009632.

692 Behara, A., Vinayachandran, P.N., 2016. An OGCM study of the impact of rain and river water
693 forcing on the Bay of Bengal. J. Geophys. Res. Oceans 121, 2425-2446.
694 doi:10.1002/2015JC011325.

695 Blanke, B., Delecluse, P., 1993. Variability of the tropical Atlantic Ocean simulated by a general
696 circulation model with two different mixed-layer physics. J. Phys. Oceanogr. 23(7), 1363-
697 1388. doi:10.1175/1520-0485(1993)023<1363:VOTTAO>2.0.CO;2.

698 Brodeau, L., Barnier, B., Treguier, A.M., Penduff, T., Gulev, S., 2010. An ERA40-based
699 atmospheric forcing for global ocean circulation models. Ocean. Model. 31(3-4), 88-104.
700 doi:10.1016/j.ocemod.2009.10.005.

701 Chaitanya, V.S., Lengaigne, M., Vialard, J., Gopalakrishna, V.V., Durand, F., Kranthikumar, C.,
702 Amritash, S., Suneel, V., Papa, F., Ravichandran, M., 2014. Salinity Measurements
703 Collected by Fishermen Reveal a "River in the Sea" Flowing Along the Eastern Coast of
704 India. Bull. Am. Meteorol. Soc. 95, 1897-1908. doi:10.1175/BAMS-D-12-00243.1.

705 Chatterjee, A., Shankar, D., Shenoi, SSC., Reddy, G.V., Michael, G.S., Ravichandran, M.,
706 Gopalkrishna, V.V., Rama Rao, E.P., Udaya Bhaskar, T.V.S., Sanjeevan, V.N., 2012. A
707 new atlas of temperature and salinity for the north Indian Ocean. J. Earth. Syst. Sci. 121(3),
708 559-593.

709 Chelton, D.B., Schlax, M.G., Samelson, R.M., 2011. Global observations of nonlinear mesoscale
710 eddies, Prog. Oceanogr., 91, 167–216, doi:10.1016/j.pocean.2011.01.002.

711 Chen, F., Mitchell, K., Schaake, J., Xue, Y., Pan, H-L., Koren, V., Duan, Q.Y., Ek, M., Betts, A.,
712 1996. Modeling of land surface evaporation by four schemes and comparison with FIFE
713 observations. J. Geophys. Res. 101(D3), 7251-7268. doi:10.1029/95JD02165.

714 Chen, G., Li, Y., Xie, Q., Wang, D., 2018. Origins of eddy kinetic energy in the Bay of Bengal. J.
715 Geophys. Res. Ocean. 123, 2097-2115. https://doi.org/10.1002/2017JC013455

716 Chou, M-D., Suarez, M.J., 1999. A solar radiation parameterization (CLIRAD-SW) developed at
717 Goddard Climate and Radiation Branch for Atmospheric Studies, Goddard Space Flight
718 Center, Greenbelt, NASA Tech. Memo. NASA/TM-1999-104606(15).

719 Dai, A., Trenberth, K.E., 2002. Estimates of freshwater discharge from continents: Latitudinal
720 and seasonal variations. J. Hydrometeorol. 3, 660-687.
721 de Boyer Montégut, C., Madec, G., Fischer, AS., Lazar, A., Iudicone, D., 2004. Mixed layer
722 depth over the global ocean: an examination of profile data and a profile-based climatology.
723 J. Geophys. Res. 109, C12003. doi:10.1029/2004JC002378.
724 de Boyer Montégut, C., Vialard, J., Shenoi, S.S.C., Shankar, D., Durand, F., Ethé, C., Madec, G.,
725 2007. Simulated Seasonal and Interannual Variability of the Mixed Layer Heat Budget in
726 the Northern Indian Ocean. J. Climate 20(13), 3249-3268. doi:10.1175/JCLI4148.1.
727 Dee, D.P., et al., 2011. The ERA-Interim reanalysis: Configuration and performance of the data
728 assimilation system. Q J Roy Meteorol Soc 137(656), 553-597. doi:10.1002/qj.828.
729 Dudhia, J., 1989. Numerical study of convection observed during the Winter Monsoon
730 Experiment using a mesoscale two-dimensional model. J. Atmos. Sci. 46, 3077-3107.
731 Durack, P.J., Wijffels, S.E., 2010. Fifty-year trends in global ocean salinities and their
732 relationship to broad-scale warming. J. Climate 23(16), 4342-4362.
733 Findlater, J., 1969. A major low-level air current near the Indian Ocean during the northern
734 summer. Q. J. Roy. Meteorol. Soc. 95, 362-380. doi: 10.1002/qj.49709540409.
735 Fournier, S.J., Vialard, J., Lengaigne, M., Lee, T., Gierach, M.M., Chaitanya, A.V.S., 2017.
736 Unprecedented satellite synoptic views of the Bay of Bengal “river in the sea”. J. Geophys.
737 Res. Ocean, online first, doi: 10.1002/2017JC013333.
738 Gadgil, S., Gadgil, S., 2006. The Indian Monsoon, GDP and Agriculture. Economic and Political
739 Weekly 41(47), 4887-4895.
740 Gadgil, S., Joshi, N.V., Joseph, P.V., 1984. Ocean-atmosphere coupling over monsoon regions.
741 Nature. 312, 141-143.
742 Girishkumar, M.S., Ravichandran, M., McPhaden, M.J., 2013. Temperature inversions and their
743 influence on the mixed layer heat budget during the winters of 2006–2007 and 2007–2008
744 in the Bay of Bengal. J. Geophys. Res. 118, 2426-2437. doi: 10.1002/jgrc.20192.
745 Graham, N.E., Barnett, T.P., 1987. Sea surface temperature, surface wind divergence and
746 convection over tropical oceans. Science. 238, 657-659. doi:10.1126/science.238.4827.657.
747 Han, W., McCreary, J.P., Kohler, K.E., 2001. Influence of precipitation minus evaporation and
748 Bay of Bengal rivers on dynamics, thermodynamics, and mixed layer physics in the upper
749 Indian Ocean. J. Geophys. Res. 106(C4),6895-6916. doi:10.1029/2000JC000403.

750 Held, I.M., Soden, B.J., 2006. Robust responses of the hydrological cycle to global warming. J.
751 Climate 19, 5686-5699.
752 Hong, S.Y., Lim, J.O.J., 2006. The WRF Single-Moment 6-Class Microphysics Scheme (WSM6)
753 J. Korean Meteor. Soc. 42, 129-151.
754 Howden, S.D., Murtugudde, R., 2001. Effects of river inputs into the Bay of Bengal. J. Geophys.
755 Res. 106(C9), 19825-19843. doi:10.1029/2000JC000656.
756 Janjić, Z.I., 1994. The step-mountain Eta coordinate model: Further developments of the
757 convection, viscous sublayer, and turbulence closure schemes. Mon. Weather Rev. 122(5),
758 927-945. doi:10.1175/1520-0493(1994)122<0927:TSMECM>2.0.CO;2.
759 Jerlov, N.G., 1968. Optical oceanography. Elsevier, London
760 Joseph, P.V., Raman, P.L., 1966. Existence of low level westerly jet-stream over peninsular India
761 during July. Indian J. Meteorol. Geophys.17, 407-410.
762 Kain, J.S., 2004. The Kain-Fritsch convective parameterization: an update. J. Appl. Meteorol. 43,
763 170-181.
764 Kumari, A., Prasanna Kumar, S., Chakraborty, A., 2018. Seasonal and Interannual Variability in
765 the Barrier Layer of the Bay of Bengal. J. Geophys. Res. Oceans 123, 1001–1015.
766 https://doi.org/10.1002/2017JC013213.
767 Li, C., Yanai, M., 1996. The onset and interannual variability of the Asian summer monsoon in
768 relation to land-sea thermal contrast. J. Climate 9, 358-375.
769 Li, Y., Han, W., Ravichandran, M., Wang, W., Shinoda, T., Lee, T., 2017. Bay of Bengal salinity
770 stratification and Indian summer monsoon intraseasonal oscillation: 1. Intraseasonal
771 variability and causes, J. Geophys. Res. Oceans 122, 4291-4311, doi:
772 10.1002/2017JC012691.
773 Lotliker, A.A., Omand, M.M., Lucas, A.J., Laney, S.R., Mahadevan, A., Ravichandran, M.,
774 2016. Penetrative radiative flux in the Bay of Bengal. Oceanography 29, 214-221.
775 Lukas, R., Lindstrom, E., 1991. The mixed layer of the western equatorial Pacific Ocean J.
776 Geophys. Res. 96(S01), 3343-3357. doi:10.1029/90JC01951.
777 Madec, G., 2008. NEMO ocean engine, Note du Pôle de modélisation, Institut Pierre-Simon
778 Laplace (IPSL), France, No 27, ISSN No 1288-1619, 2008.
779 Masson, S., et al., 2005. Impact of barrier layer on winter–spring variability of the southeastern
780 Arabian Sea. Geophys. Res. Lett. 32, L07703. doi:10.1029/2004GL021980p.

781 Mignot, J., de Boyer Montégut, C., Lazar, A., Cravatte, S., 2007. Control of salinity on the mixed
782 layer depth in the world ocean: 2. Tropical areas, J. Geophys. Res. 112, C10010.
783 doi:10.1029/2006JC003954.
784 Mlawer, E.J., Taubman, S.J., Brown, P.D., Iacono, M.J., Clough, S.A., 1997. Radiative transfer
785 for inhomogeneous atmospheres: RRTM, a validated correlated-k model for the longwave,
786 J. Geophys. Res. 102(D14), 16663-16682. doi:10.1029/97JD00237.
787 Noh, Y., Cheon, W.G., Hong, S.Y., Raasch, S., 2003. Improvement of the K-profile model for
788 the planetary boundary layer based on large eddy simulation data. Bound. Lay. Meteorol.
789 107(2), 401-427. doi:10.1023/A:1022146015946.
790 Praveen Kumar, B., Vialard, J., Lengaigne, M., Murty, V., McPhaden, M., 2012. Tropflux: air-
791 sea fluxes for the global tropical oceans–description and evaluation. Clim. Dyn. 38, 1521-
792 1543. doi:10.1007/s00382-011-1115-0.
793 Praveen Kumar, B., Vialard, J., Lengaigne, M., Murty, V., McPhaden, M., Cronin, M., Pinsard,
794 F., Reddy, K.G., 2013. Tropflux wind stresses over the tropical oceans: Evaluation and
795 comparison with other products. Clim. Dyn. 40, 2049. https://doi.org/10.1007/s00382-012-
796 1455-4.
797 Rao, R.R., Sivakumar, R., 2003. Seasonal variability of sea surface salinity and salt budget of the
798 mixed layer of the north Indian Ocean, J. Geophys. Res. 108(C1), 3009.
799 doi:10.1029/2001JC000907.
800 Samson, G., Masson, S., Lengaigne, M., Keerthi, M.G.., Vialard, J, Pous, S., Madec, G.,
801 Jourdain, N.C., Jullien, S., Menkes, C., Marchesiello, P., 2014. The NOW regional coupled
802 model: Application to the tropical Indian Ocean climate and tropical cyclone activity. J.
803 Adv. Model. Earth Syst. 6, 700-722. doi:10.1002/2014MS000324.
804 Sengupta, D., Bharath Raj, G.N., Shenoi, S.S.C., 2006. Surface freshwater from Bay of Bengal
805 runoff and Indonesian throughflow in the tropical Indian Ocean. Geophys. Res. Lett. 33,
806 L22609. doi:10.1029/2006GL027573.
807 Sengupta, D., Bharath Raj, N., Ravichandran, M., Sree Lekha, J., Papa, F., 2016. Near-surface
808 salinity and stratification in the north Bay of Bengal from moored observations. Geophys.
809 Res. Lett. 43, 4448-4456. doi:10.1002/2016GL068339.
810 Seo, H., Xie, S., Murtugudde, R., Jochum, M., Miller, A.J., 2009. Seasonal effects of Indian
811 Ocean freshwater forcing in a regional coupled model. J. Climate 22, 6577-6596.

812 Shenoi, S.S.C., Shankar, D., Shetye, S.R., 2002. Differences in heat budgets of the near-surface
813 Arabian Sea and Bay of Bengal: Implications for the summer monsoon. J. Geophys. Res.
814 107(C6), 1-14.
815 Skamarock, W.C., Klemp, J.B., 2008. A Time-Split Nonhydrostatic Atmospheric Model for
816 Weather and Forecasting Applications. J. Comp. Phys. 227, 3465-3485,
817 doi:10.1016/j.jcp.2007.01.037.
818 Sprintall, J., Tomczak, M., 1992. Evidence of the barrier layer in the surface layer of the tropics,
819 J. Geophys. Res. 97(C5), 7305-7316.
820 Thadathil, P., Muraleedharan, P.M., Rao, R.R., Somayajulu, Y.K., Reddy, G.V.,
821 Revichandran, C., 2007. Observed seasonal variability of barrier layer in the Bay of
822 Bengal, J. Geophys. Res. 112, C02009, doi:10.1029/2006JC003651.
823 Thadathil, P., Suresh, I., Gautham, S., Prasanna Kumar, S., Lengaigne, M., Rao, R.R., Neetu, S.,
824 Hegde, A., 2016. Surface layer temperature inversion in the Bay of Bengal: Main
825 characteristics and related mechanisms. J. Geophys. Res. Oceans 121, 5682–5696,
826 doi:10.1002/2016JC011674.
827 Valcke, S., 2013. The OASIS3 coupler: A European climate modelling community software,
828 Geosci. Model. Dev. 6(2), 373–388, doi:10.5194/gmd-6-373-2013.
829 Vialard, J., Delecluse, P., 1998. An OGCM Study for the TOGA Decade. Part I: Role of Salinity
830 in the Physics of the Western Pacific Fresh Pool. J. Phys. Oceanogr. 28(6), 1071-1088.
831 doi:10.1175/1520-0485(1998)028<1071:AOSFTT>2.0.CO;2.
832 Vialard, J., Menkes, C., Boulanger J.P., Delecluse P., Guilyardi, E., McPhaden, M.J., Madec, G.,
833 2001. A model study of oceanic mechanisms affecting equatorial Pacific sea surface
834 temperature during the 1997-98 El Niño. J. Phys. Oceanogr. 31(7), 1649-1675.
835 Vinayachandran, P.N.., Jahfer, S., Nanjundiah, R.S., 2015. Impact of river runoff into the ocean
836 on Indian summer monsoon. Environ. Res. Lett. 10(5), 054008. doi:10.1088/1748-
837 9326/10/5/054008.
838 Vinayachandran, P.N., Murty, V.S.N., Ramesh Babu, V., 2002. Observations of barrier layer
839 formation in the Bay of Bengal during summer monsoon. J. Geophys. Res. 107(C12), 8018,
840 doi:10.1029/2001JC000831.
841 Vinayachandran, P.N., Shankar, D., Kurian, J., Durand, F., Shenoi, S.S.C., 2007. Arabian Sea
842 mini warm pool and the monsoon onset vortex. Current Sci. 93(2), 203-214.
843 Webster, P.J., Magana, V.O., Palmer, T.N., Shukla, J., Tomas, R.A., Yanai, M., Yasunari, T.,

1998. Monsoons: Processes, predictability and prospects for prediction. J. Geophys. Res. 103 (C7), 14451-14510.

Wijesekera, H.W., et al., (2016) ASIRI: an ocean–atmosphere initiative for Bay of Bengal. Bull. Am. Meteorol. Soc. 97(10), 1859-1884.

852
853
854

Experiment name	Purpose
CTL	Reference experiment. See text for details on resolution & configuration.
NOS	As CTL but with no impact of salinity on vertical mixing.
FCTL	As CTL, but with wind stress correction over the Bay of Bengal.
FNOS	As FCTL, but with no impact of salinity on vertical mixing.
CTL-NSP	As CTL, but with no solar flux penetration into the ocean.
NOS-NSP	As CTL_NSP, but with no impact of salinity on vertical mixing.
CTL-G	As CTL, but using Goddard shortwave radiation scheme.
NOS-G	As NOS, but using Goddard shortwave radiation scheme.
CTL-KF	As CTL, but using Kain-Fritsch sub-grid atmospheric convection scheme.
NOS-KF	As NOS, but using Kain-Fritsch sub-grid atmospheric convection scheme.

855

856 **Table 1:** NOW (NEMO-Oasis-WRF) regional coupled model experiments used in this study.

857
858
859
860

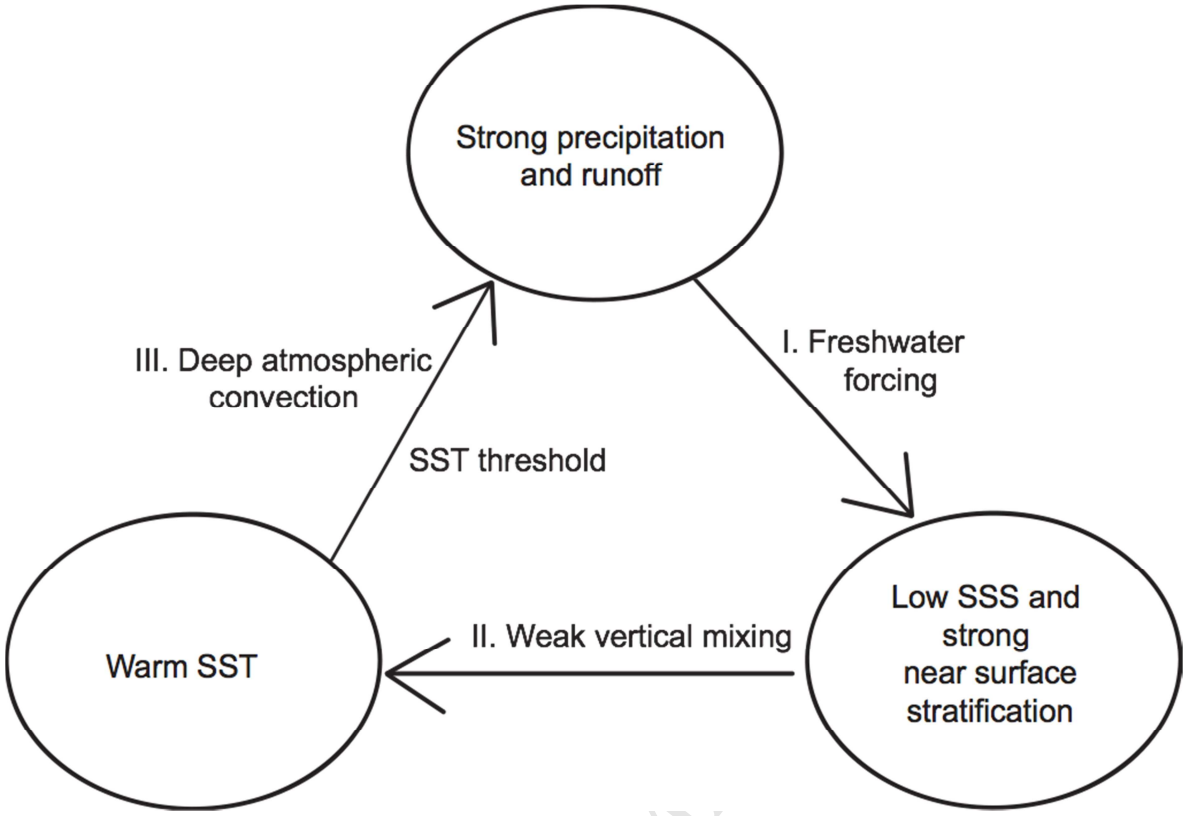

861

862 **Figure 1:** Sketch of the positive feedback mechanism proposed by Shenoi et al. (2002), by which
863 the BoB haline stratification could sustain enhanced regional precipitation.

864

865

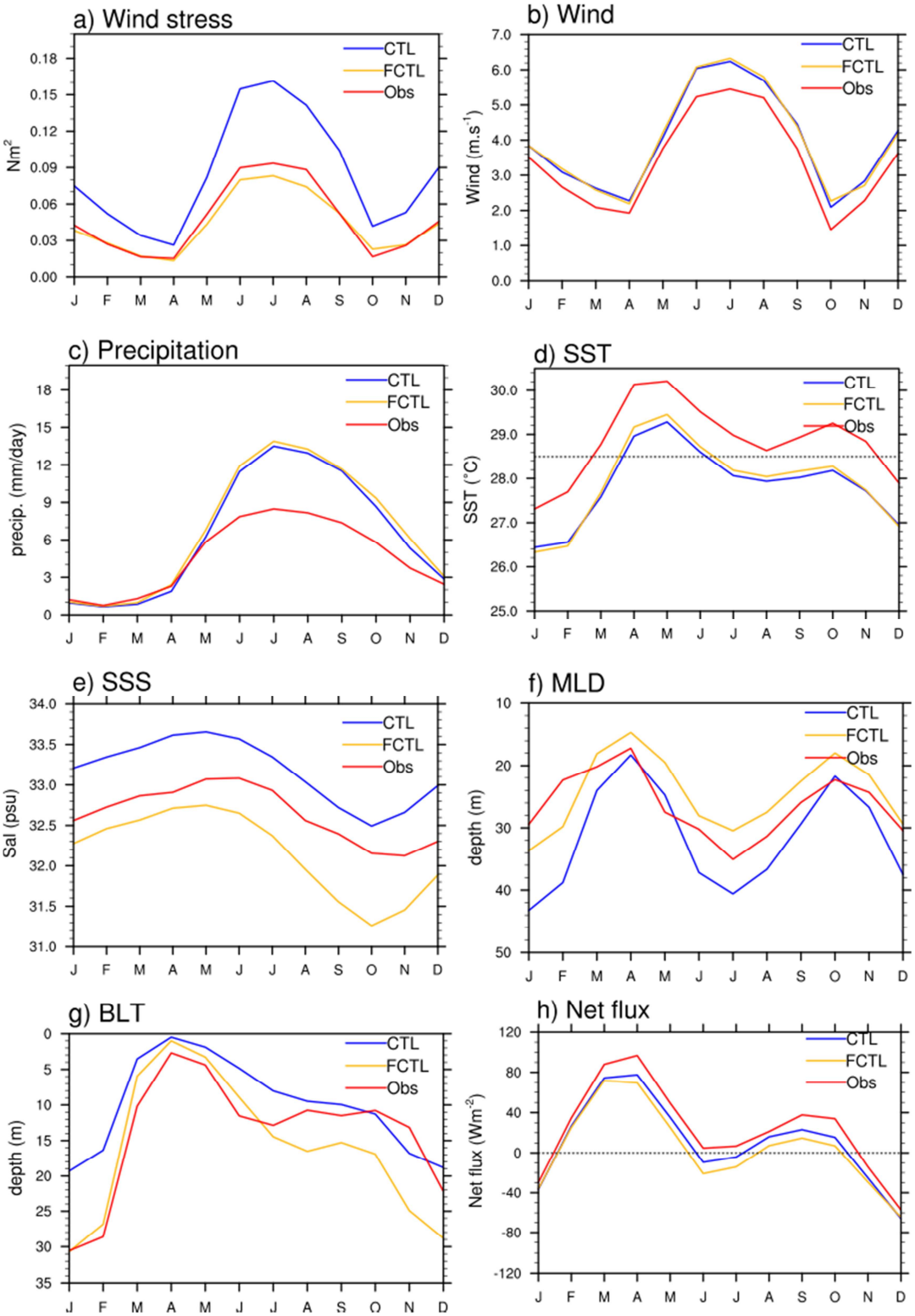
a) Wind stress
Nm^2
CTL
FCTL
Obs
b) Wind
Wind (m.s^{-1})
c) Precipitation
precip. (mm/day)
d) SST
SST (°C)
e) SSS
Sal (psu)
f) MLD
depth (m)
g) BLT
depth (m)
h) Net flux
Net flux (Wm^{-2})
J F M A M J J A S O N D

866

867 **Fig. 2** Averaged BoB (6°N-25°N, 80°E-100°E, see region on Fig. 3) climatological seasonal
868 cycle for CTL (Blue) & FCTL (flux correction applied on wind stress: see text for details,
869 yellow) experiments and observations (red) for **(a)** wind stress ($N.m^{-2}$), **(b)** wind speed ($m.s^{-1}$) **(c)**
870 precipitation ($mm.day^{-1}$) ($W.m^{-2}$), **(d)** Sea Surface Temperature (SST, °C), **(e)** Sea Surface
871 Salinity (SSS, pss), **(f)** mixed layer depth (MLD, m) **(g)** Barrier Layer Thickness (BLT, m) and
872 **(h)** net heat flux. Observed climatologies are obtained from the TropFlux 1990-2007 average for
873 wind stress and net heat flux, ERA-interim 1990-2007 average for wind speed, TMI 1998-2006
874 average for SST, TRMM 1998-2011 average for rainfall, NIOA climatology for SSS and de
875 Boyer Montegut et al. (2004) climatology for MLD and BLT. The dashed horizontal line on
876 panel d indicates the observed threshold (28.5°C) for deep atmospheric convection.

877

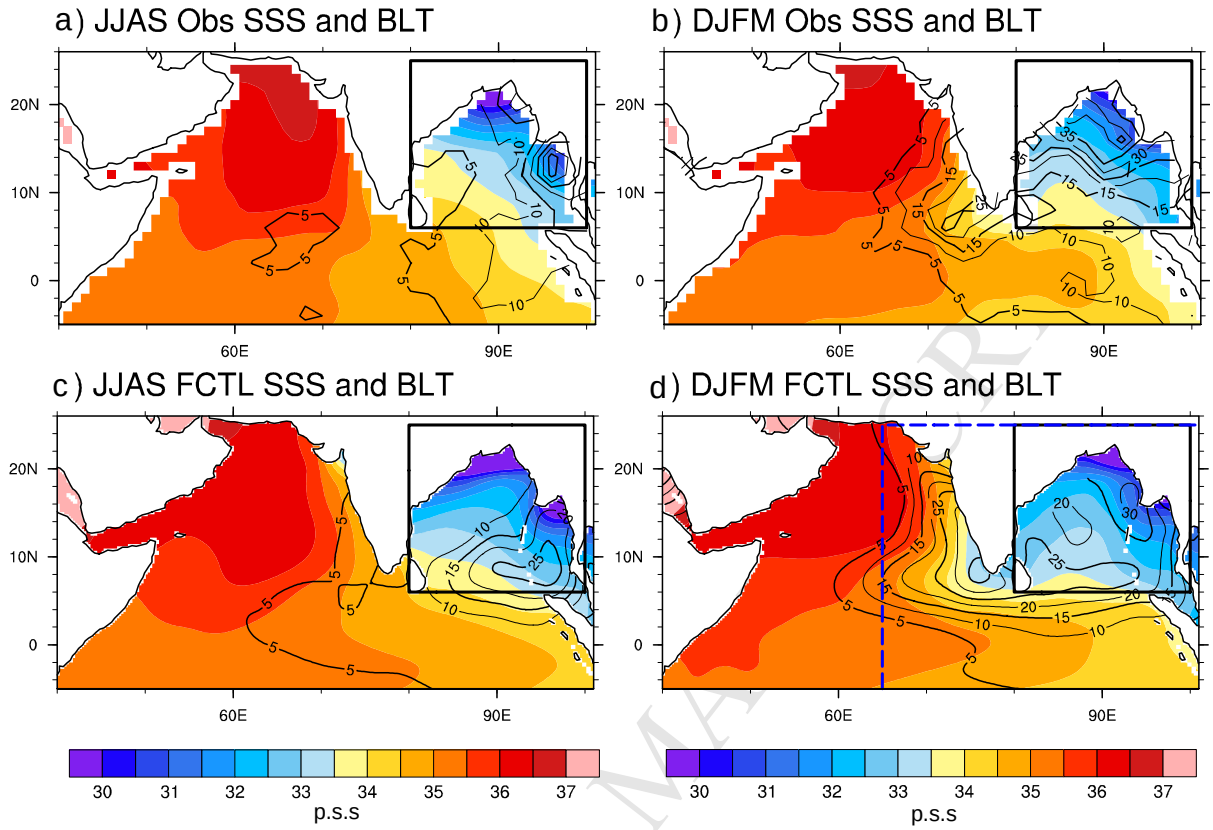

878

879 **Fig. 3** Summer (June to September: JJAS) (**left**) and Winter (December to March; DJFM) (**right**)
880 climatologies of observation (**top**) and FCTL (**bottom**) Sea Surface Salinity (SSS, shading, pss)
881 and Barrier Layer Thickness (BLT, contours, meters). For the model data, a horizontal smoothing
882 has been applied, with a similar spatial scale than that used for the observationally-derived
883 climatologies i.e. with a smoothing radius of 175 km for BLT as for de Boyer Montegut et al.
884 (2004) and 4° (444 km) for SSS as for the NIOA climatology. The dashed blue frame on panel d
885 indicates the region over which the influence of salinity on vertical mixing is neglected in the
886 series of "NOS" experiments (see table 1).

887

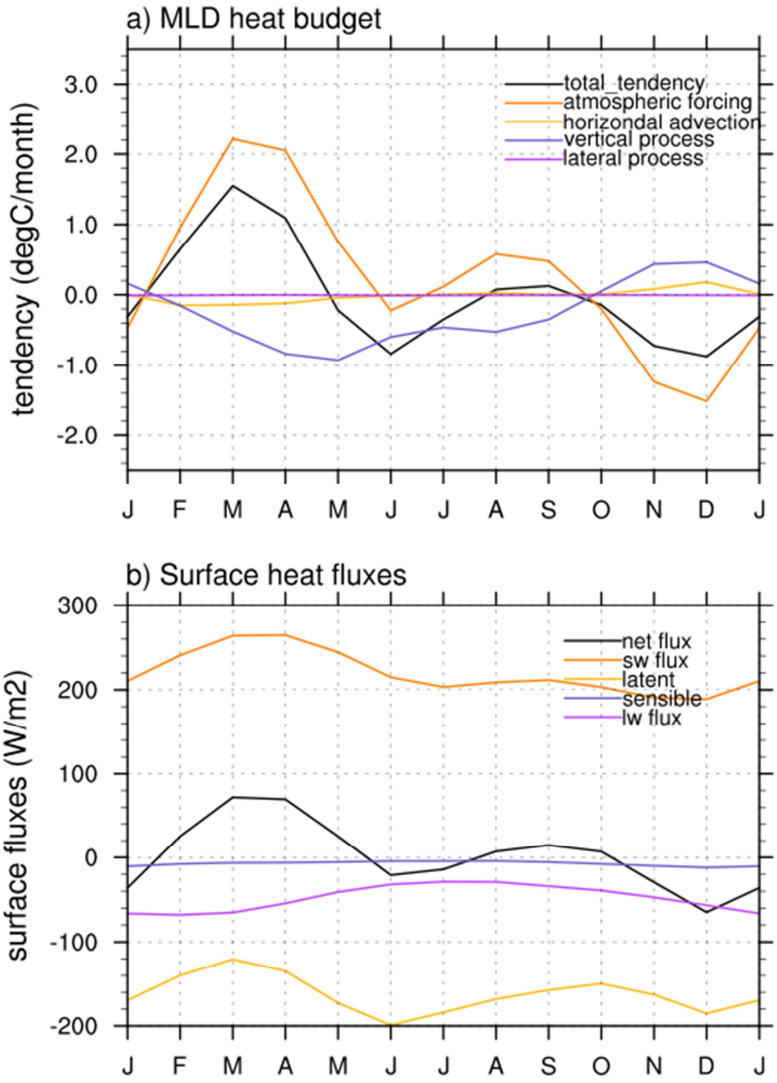

888

889 **Figure 4.** Averaged BoB climatological seasonal cycle of FCTL **(a)** mixed layer heat budget
890 terms (°C.month^{-1}, see section 2.3 for details) and **(b)** surface net heat fluxes and its four
891 components (W.m^{-2}).

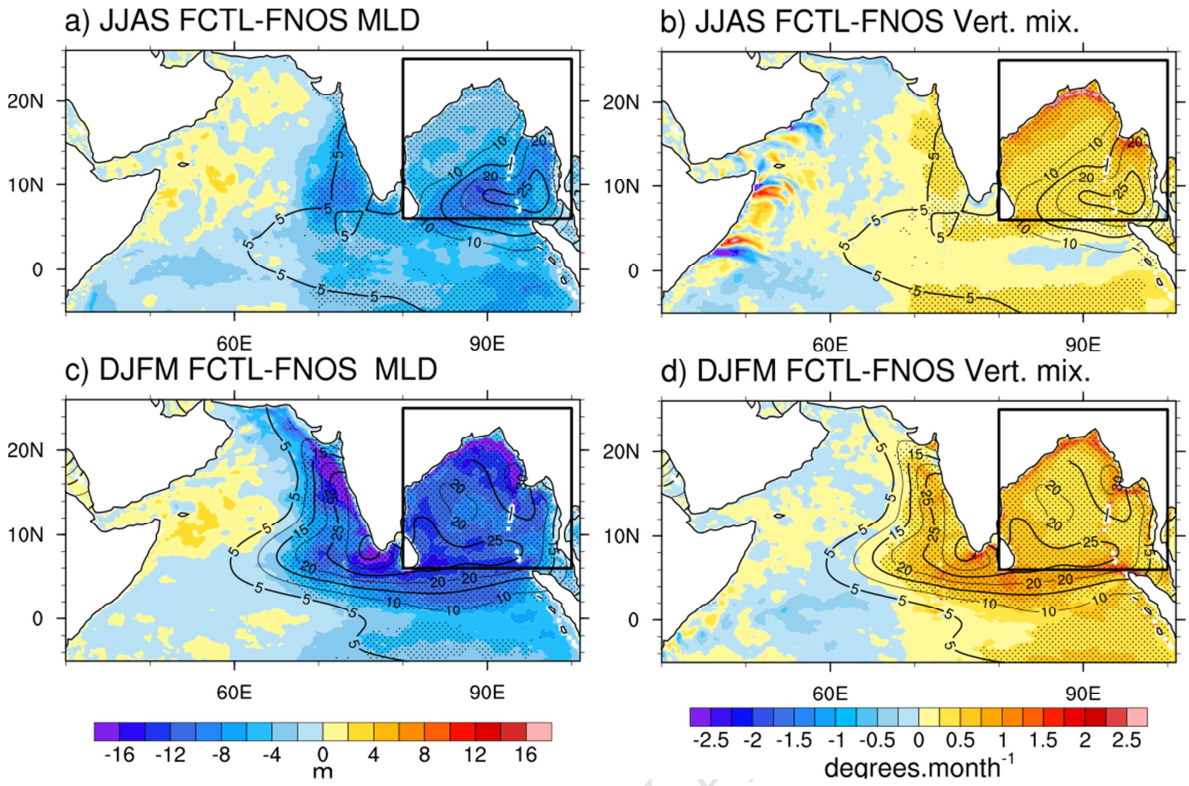

892

893 **Figure 5. (Top)** Summer (JJAS) and **(bottom)** winter (DJFM) climatological maps of FCTL
894 minus FNOS **(left)** mixed layer depth (m) and **(right)** vertical mixing term of the mixed layer
895 heat budget (°C.month^{-1}). The FCTL run climatological barrier layer thickness is overlaid as
896 contours. Dots indicate regions for which MLD (left) and vertical mixing (right) differences
897 between the FCTL and FNOS simulations are significantly different from zero at the 95%
898 confidence level (using a one-tailed student's t-test with degrees of freedom equal to number of
899 years minus one).

900

901

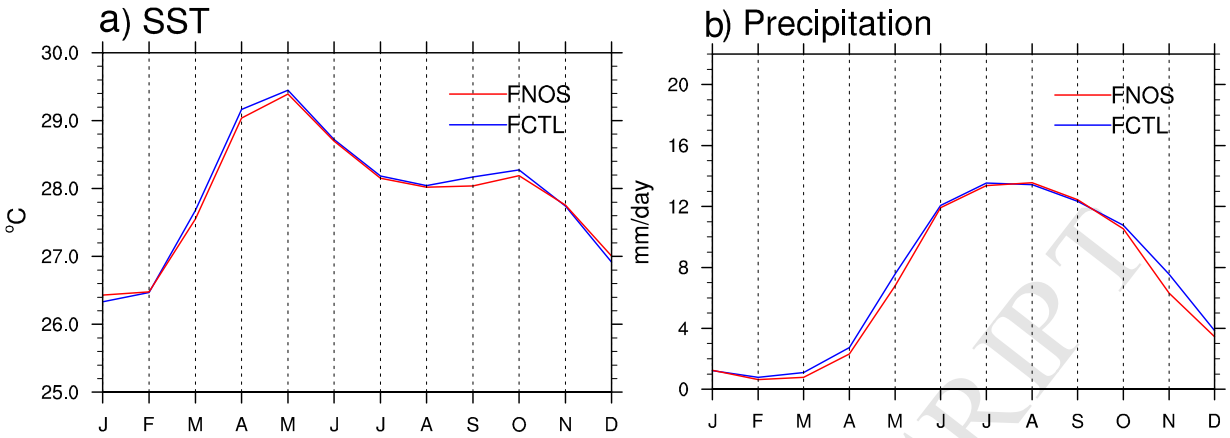

902

903 **Figure 6.** Average BoB FCTL and FNOS **(e)** SST and **(f)** precipitation climatological seasonal
904 cycle.

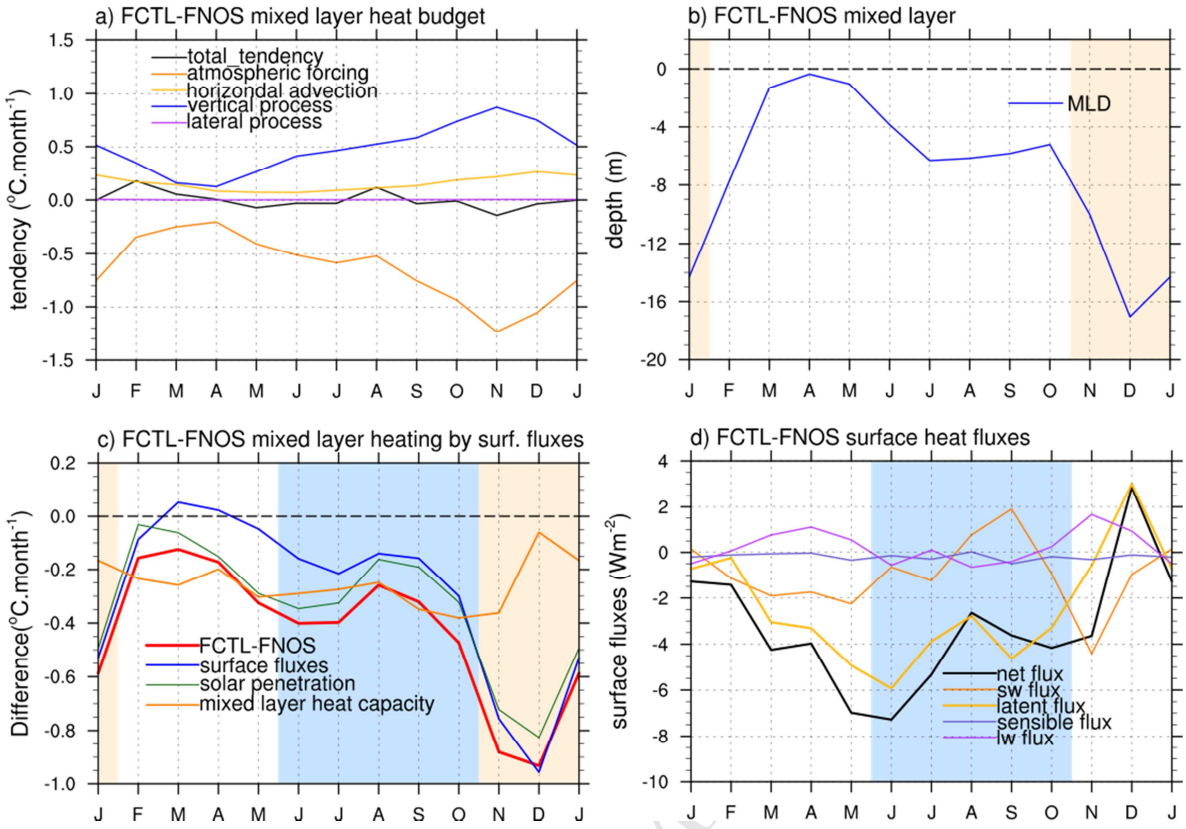

Figure 7. Average BoB climatological seasonal cycle of FCTL minus FNOS **(a)** MLD heat budget (°C.month^{-1}), **(b)** MLD (m) and **(d)** surface fluxes (W.m^{-2}). **(c)** shows the FCTL minus FNOS recomputed atmospheric forcing term (thick red curve). The green curve allows to evaluate the effect of solar penetration, the blue curve the effect of the change in surface heat fluxes and the orange one the effect of the changes in mixed layer heat capacity (see text and Annex A for details). The blue shading highlights the July to October period and the salmon shading highlights the November to January period.

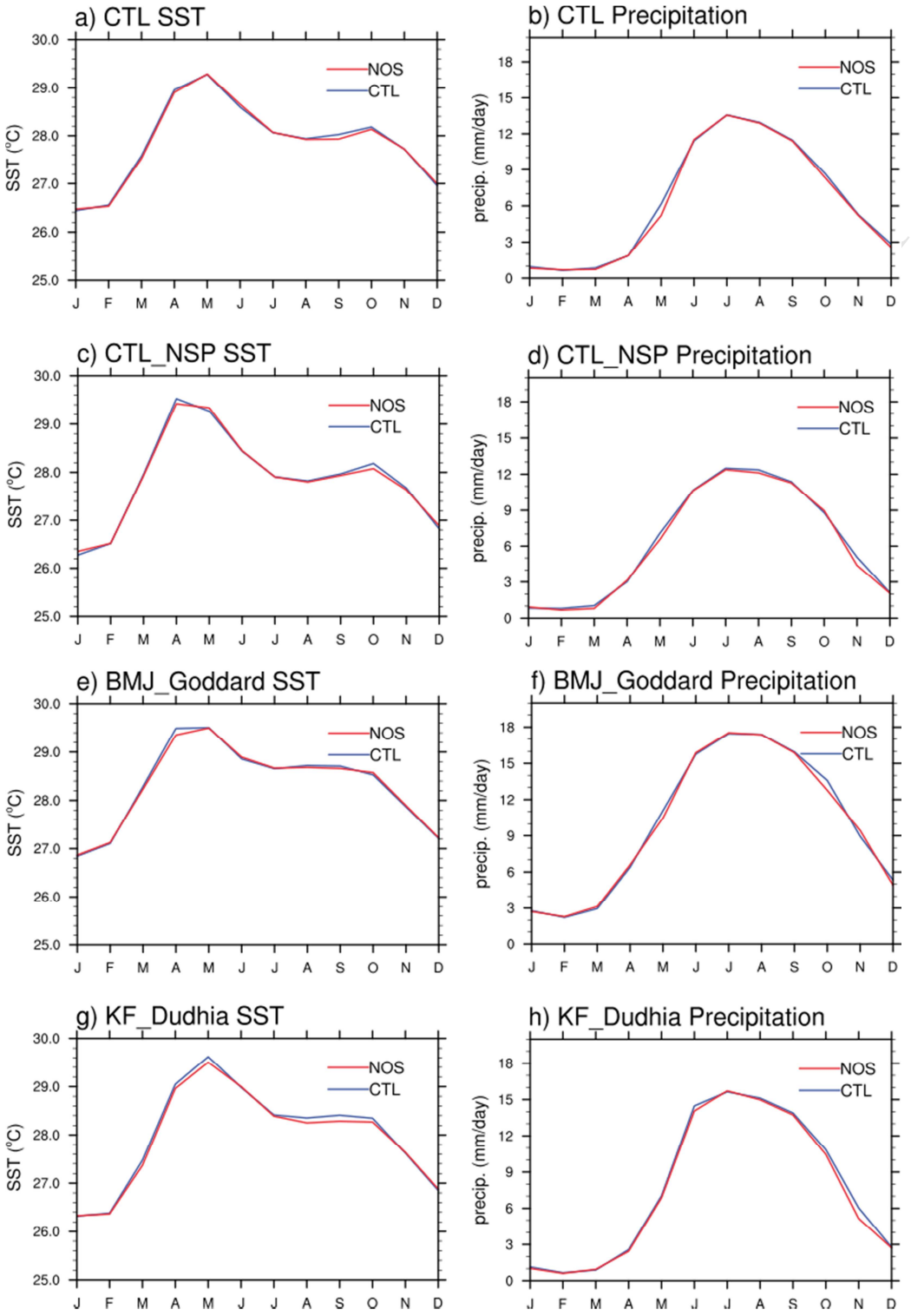

Fig. 8: Averaged BoB CTL and NOS mean seasonal cycle of **(a)** SST and **(b)** precipitation (i.e. same as 8ef but without flux corrections). **(c)-(d)** Same as **(a)-(b)**, but for CTL-NSP and NOS-NSP (i.e. with the penetration of solar radiation into the ocean de-activated). **(e)-(f)** Same as **(a)-**

917 **(b)**, but for CTL-G and NOS-G (Goddard shortwave radiation parameterization). **(g)-(h)** Same as
918 **(a)-(b)**, but for CTL-KF and NOS-KF (Kain-Fritsch convective parameterization).

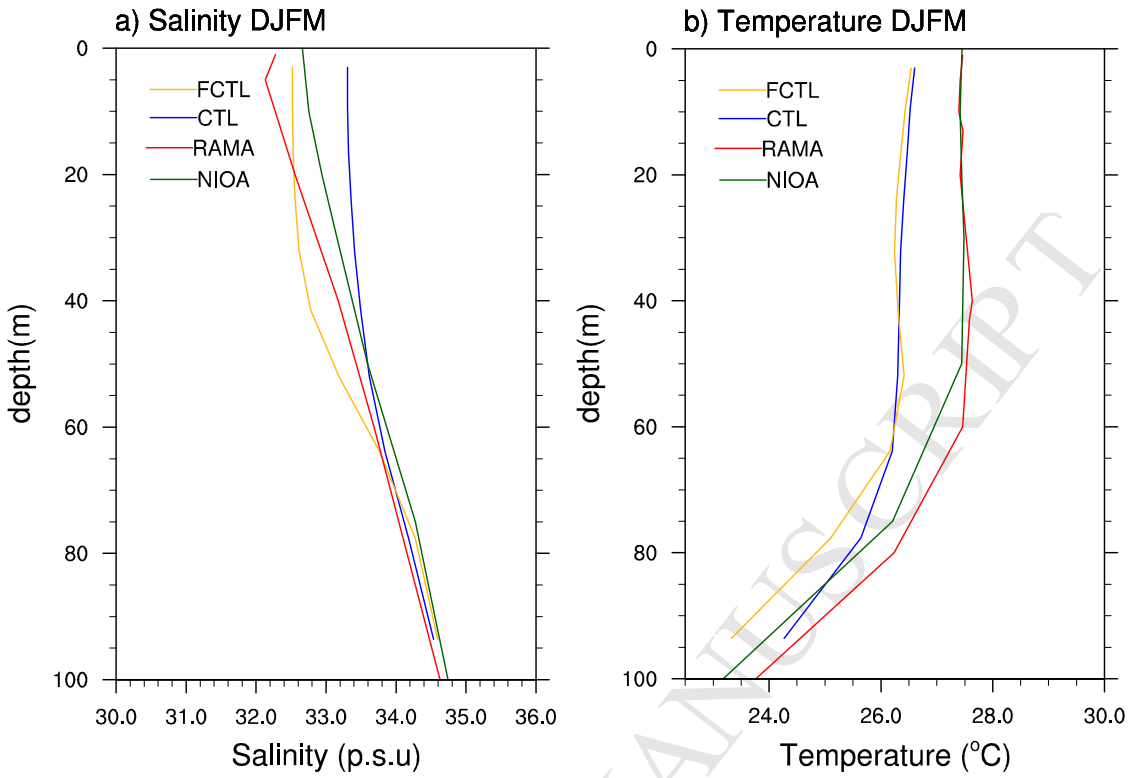

919

920 **Fig 9.** Winter (DJFM) temperature and salinity BoB-averaged climatological profiles for
921 longitude 90°E and latitude 15°N from the RAMA buoy (red), NIOA product (green), CTL (blue)
922 and FCTL (yellow).

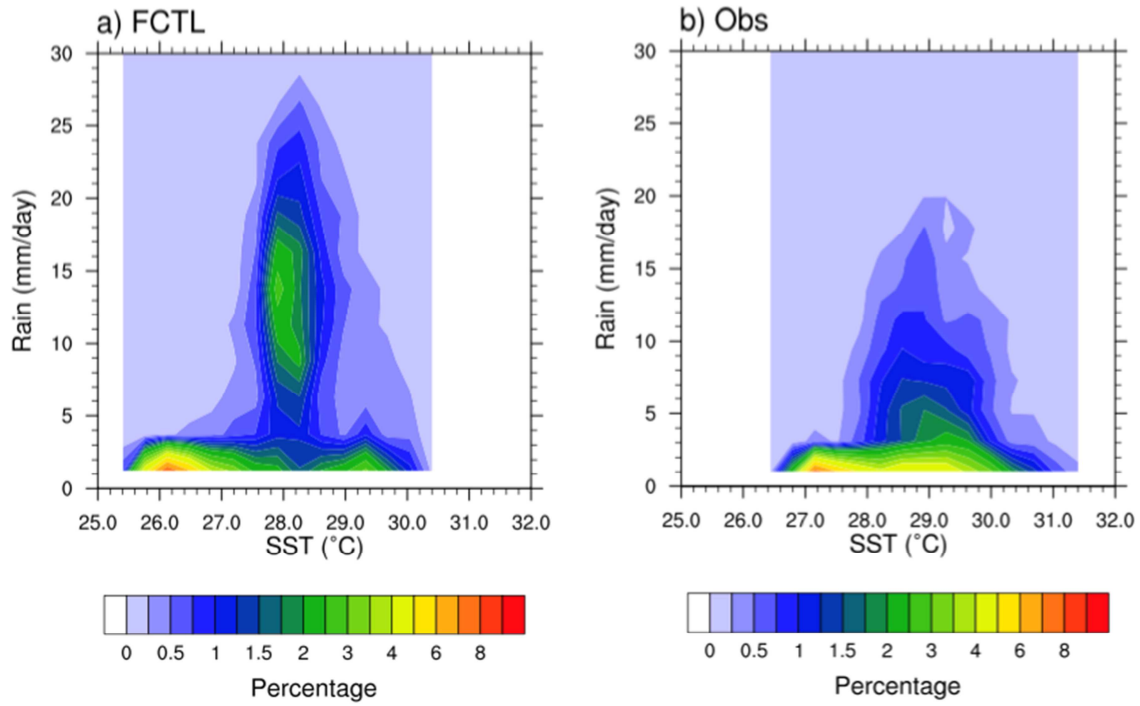

923

924 **Figure 10:** SST-rainfall relation in **(a)** the FCTL simulation and **(b)** from TMI and TRMM
925 observations. The probability density function (%) was constructed from daily SST and rainfall
926 over the BoB region, using 2.5 mm.day^{-1} and 0.33°C wide bins.